frontiers | Frontiers in Acoustics

TYPE Review
PUBLISHED 19 November 2024
DOI 10.3389/facou.2024.1483731



OPEN ACCESS

EDITED BY
Yun Jing,
The Pennsylvania State University (PSU), United States

REVIEWED BY
Mitra Aliabouzar,
University of Michigan, United States
Dingjie Suo,
Beijing Institute of Technology, China

*CORRESPONDENCE
Sevan Harput,
harputs@lsbu.ac.uk

RECEIVED 20 August 2024
ACCEPTED 01 November 2024
PUBLISHED 19 November 2024

CITATION
Dorvashi M, Harrison OJ, Sultan HH, Zhang G, Thanou M, Ghavami N, Tiberi G, Ghavami M and Harput S (2024) A meta-analysis of the effect of ultrasound activation parameters on phase-change nanodroplets in imaging and therapy. *Front. Acoust.* 2:1483731.
doi: 10.3389/facou.2024.1483731



# A meta-analysis of the effect of ultrasound activation parameters on phase-change nanodroplets in imaging and therapy

Maryam Dorvashi[1], Owen J. Harrison[2], Hossam H. Sultan[1], Ge Zhang[3], Maya Thanou[2], Navid Ghavami[4], Gianluigi Tiberi[1,4], Mohammad Ghavami[1] and Sevan Harput[1]*

[1]South Bank Applied Bioengineering Research, London South Bank University, London, United Kingdom, [2]Institute of Pharmaceutical Sciences, School of Cancer and Pharmaceutical Sciences, King's College London, London, United Kingdom, [3]INSERM U1273 Physics for Medicine Paris (ESPCI), Paris, France, [4]Umbria Bioengineering Technologies Srl, Perugia, Italy

Phase-change nanodroplets (PCNDs) have been used in ultrasound imaging, targeted drug delivery, blood-brain-barrier (BBB) opening, sonothrombolysis and histotripsy for over a decade. For these ultrasound applications, PCNDs provide higher *in vivo* lifetime than microbubbles (MBs), the potential for extravasation inside tumour and on demand activation, which is the transition of the liquid-core of nanodroplets to gaseous microbubbles through acoustic droplet vaporisation (ADV). Operating above the ADV threshold can offer repeatable activation of PCNDs and the subsequent oscillation of acoustically activated PCNDs, which is advantageous in imaging and therapeutic applications. Efficient and repeatable activation of PCNDs require a good understanding of ultrasound parameters and nanodroplet composition for different biomedical applications. Therefore, this article presents a meta-analysis of the effect of ultrasound activation parameters on ADV for various PCNDs in different biomedical applications. About 7,500 articles were considered for this study, but only 45 articles were chosen and evaluated in the meta-analysis based on the following criteria: 1): activation parameters, including ultrasound frequency, peak negative pressure, transmit pulse length or duration have been clearly mentioned, 2), droplets range in nanometre size (<1 μm), 3), experiments are performed at a temperature of 37°C and 4) ADV threshold has been clearly mentioned and observations are not due to inertial cavitation (IC). From selected publications, we recorded the activation frequency (0.06–16 MHz), ultrasound pressure (0.18–14.9 MPa), activation pulse length (μs-ms range) and nanodroplet size for different types of perfluorocarbon PCNDs ($C_3F_8$, $C_4F_{10}$, $C_5F_{12}$ and $C_6F_{14}$) and evaluated the relation of these parameters to each other. Finally, a Root Mean Square (RMS)-like power metric, which is a combination of ultrasound peak negative pressure and square root of ultrasound pulse length, is proposed for identifying the ADV threshold behaviour instead of using pressure or mechanical index values.

KEYWORDS

**phase change nanodroplets, acoustic droplet vaporization (ADV), ultrasound activation, ultrasound imaging, ultrasound therapy, microbubbles**

# 1 Introduction

Ultrasound waves have been used in imaging and therapeutic applications for more than 60 years (Kee and Teo, 2019; Izadifar et al., 2020; Riemer et al., 2022). In imaging, ultrasound waves generate reflections and scattering while propagating through tissue, which is then received by the ultrasound probe and used to form an image. In therapy, ultrasound waves pass through tissue and result in changes to cell membranes by boosting temperature due to absorption and cavitation following local pressure changes (Stride and Coussios, 2010; Harput et al., 2023). Although ultrasound imaging and therapy can be performed without contrast or therapeutic agents, they are often used to improve imaging performance or therapeutic efficacy.

Microbubbles (MBs), micrometre-sized gas-filled bubbles, are clinically approved ultrasound contrast agents (UCAs), which have been designed for use as ultrasonic imaging contrast agents and disease diagnosis (Stride and Coussios, 2010). While oscillation of UCAs under low amplitude ultrasound (mechanical index (MI) <0.7) simply generates an acoustic signal for improving image contrast, strong ultrasound fields (MI > 0.7) create shear forces which in turn elicits a multitude of bioeffects, including sonoporation (ultrasound-mediated cell permeabilisation) and increased risk of cavitation (Sen et al., 2015; Pellerito and Polak, 2012; Canavese et al., 2018). MBs are composed of a gaseous core and a lipid, protein, polymer, or surfactant shell. MBs are clinically approved UCAs and commonly used for imaging and therapeutic applications (Izadifar et al., 2020). MBs are around 1–10 μm, which restrict their distribution in the vascular space and prevents extravasation (Paproski et al., 2014). After injection to the bloodstream MBs stay in circulation for minutes (half-life of 3–15 min) *in vivo* (Liu et al., 2017) and they are rapidly cleared from the body via the liver (Mannaris et al., 2019; Navarro-Becerra et al., 2022). In addition, MBs rely on blood flow for movement throughout the vascular space which increases acquisition times for ultrasound localization microscopy in the smallest, low flow microvessels. Furthermore, due to low separation of MBs signal from tissue, detection of MBs in low-flow regions is demanding (Burgess et al., 2022).

Phase-change nanodroplets (PCNDs) have been developed in the last 2 decades to overcome the aforementioned problems (Mannaris et al., 2019). PCNDs have emerged as a switchable, intermittent, or persisting contrast agent for ULM via acoustic droplet vaporisation (ADV). PCNDs are composed of a shell and a liquid perfluorocarbon (PFC) core and are usually 10-fold smaller than MBs (Ninomiya et al., 2014). PCNDs have a longer circulation time *in vivo* as their liquid core prevents gas dissolution. PCNDs have deep penetration into the tissues via the extravascular space and passively accumulate in tumour tissue due to their nano-(15) scale size and EPR (Enhanced Permeability and Retention) effect (Ho and Yeh, 2017). PCNDs have a variety of potential applications ranging from diagnostic to therapeutic applications. The combination of PCNDs with ultrasound technology generates local cavitation which can be utilised for image contrast enhancement, tumour ablation and release of therapeutic agents loaded in PCNDs (Aliabouzar et al., 2018). Understanding how ultrasound parameters and other experimental factors affect PCND activation and ADV threshold is critical and will provide an overall insight to researchers for designing and planning experiments for specific applications. Firstly, this article will briefly explain chemical composition and fabrication techniques of PCNDs and their applications in the context of ADV. Secondly, this article will present a meta-analysis of the effect of ultrasound activation parameters of various PCNDs on the ADV threshold in different biomedical applications on the ADV threshold.

## 1.1 Chemical components of nanodroplets

PCNDs are composed of two parts, a shell and a liquid PFC core. The shell maintains the shape and original diameter of nanodroplets after intravenous injections, later expanding into bubbles following ADV (Aliabouzar et al., 2018; Borden et al., 2020). Control of ADV is in part due to the surface tension at the interface between the shell and core, providing enough Laplace pressure to prevent immediate vaporisation of low-boiling point PFCs, in turn delaying collapse/expansion of PCNDs at physiological temperatures until ultrasound is applied (Kee and Teo, 2019). As a result of these compositional and physicochemical properties, PCNDs exhibit greater stability and longer circulation time *in vivo* compared to MBs (Zhang W. et al., 2023).

### 1.1.1 Shell composition

An important aspect of nanodroplet fabrication is the shell composition. In order to find a balance between mechanical resistance (by providing enough Laplace pressure and enabling deformation during activation by energy), common shell materials include albumin, lipids, surfactants, and synthetic polymers (Lea-Banks et al., 2019). While lipids and surfactants are soft-shell materials, polymers and proteins are considered as hard-shell materials (Melich et al., 2020). Lipids and polymers are the most common material used in PCNDs formulation (Melich et al., 2020). Albumin is an emerging shell molecule for fabrication of both MB and PCND formulations due to its stabilising properties (Kripfgans et al., 2000). Bovine serum albumin is commonly used and is mostly prepared through sonication methods (Sirsi and Borden, 2009). Although the preparation of an albumin shell is relatively straight-forward, it is still more rigorous than other materials (Sheeran et al., 2016).

Lipids such as liposomes are frequently utilised in the fabrication of PCNDs due to elasticity (Schad and Hynynen, 2010; Kawabata et al., 2005) and mechanical flexibility. These properties contribute to repeated expansion and collapse of PCNDs shells which stabilises nanodroplets against dissolution and coalescence (Sheeran et al., 2016). Lipid-shelled PCNDs are commonly coated with hydrophilic poly (ethylene oxide) (PEG) chains. PEGylated lipid shell reduces the average size and size variation of PCNDs, in addition to reducing PCNDs aggregation (Yarmoska et al., 2019).

Surfactants have been used to form stable MBs, though fluorosurfactants are more suitable to form PCNDs' shells (Melich et al., 2020) as they provide appropriate stabilisation against coalescence phenomena (Melich et al., 2020). Use of polymers as the shell material provides high drug loading efficiency (Lea-Banks et al., 2019), as well as enhance intracellular drug delivery and ultrasound contrast properties (Rapoport et al., 2013; Li et al., 2020). PEG is a common

polymer utilised in combination with other polymers for size reduction and targeted drug delivery. Many studies show that polymer-coated PCNDs have better storage stability and polydispersity when compared to lipid shell (DPPC, DSPE-PEG2000, DPPG, DPPE, and cholesterol) nanodroplets (Melich et al., 2020). Also, polymer-coated PCNDs have higher vaporisation thresholds and need higher ultrasound energy for vaporisation and activation due to the stiffness of the polymer material (Cao et al., 2018). Coating material of PCNDs which has been maintained after ADV, lead to a lower surface tension, and increase in the likelihood of recondensation after ADV rather than dissolution. The present amount of coating material after ADV of PCNDs (which is difficult to quantify) decreases the surface tension and has a notable effect on the acoustic properties and stability of recondensed or vaporised PCNDs. Further studies are required to quantify changes to the coating material and surface structure of PCNDs following vaporisation/recondensation (Burgess et al., 2022).

### 1.1.2 Core composition

The preferable criteria for the liquid core of nanodroplets are hydrophobic, bioinert, and with an appropriate boiling point and safe circulation in the body before vaporisation. PFC as nanodroplet core meet these criteria (Kee and Teo, 2019). PFC formed from carbon and fluorine atoms configured into long chains. The PFC family differs in configuration and chain length (number of carbons), resulting in unique molecular weight, densities, and boiling points (Lea-Banks et al., 2019). Longer chain length correlates with higher boiling points (Lea-Banks et al., 2019; Lacour et al., 2018). Some common PFC nanodroplets are $C_3F_8$, $C_4F_{10}$, $C_5F_{12}$ and $C_6F_{14}$.

$C_5F_{12}$ (29°C boiling point) was utilised as a first-ever studied droplet core from the early 2000s (Kripfgans et al., 2000; Schad and Hynynen, 2010; Giesecke and Hynynen, 2003; Williams et al., 2013; Zhang and Porter, 2010) due to its lower boiling point than body temperature and the existence of Laplace pressure (Wong et al., 2011), resulting in greater stability in the body and free circulation *in vivo* until activation by energy. Other PFCs provide other advantages. Highly volatile PFCs including $C_4F_{10}$ (−2°C boiling point) and $C_3F_8$ (−39°C boiling point) were used for applications requiring droplets with a size below 200 nm in order to passively accumulate in the targeted tumour tissue through the leaky vessels (Sheeran et al., 2013a; Vlaisavljevich et al., 2013). Additionally, some research showed that a combination of different PFCs would reduce the vaporisation threshold and maximise the performance for specific applications (Sheeran and Dayton, 2014). A mixture of $C_5F_{12}$ (29°C boiling point) and $C_6F_{14}$ (56°C boiling point) showed that vaporisation of $C_5F_{12}$ acted as a trigger to induce vaporisation of higher boiling point $C_6F_{14}$ (Fix et al., 2017). Currently, most of the studies have focused on PCNDs with a single-type of PFC core, whilst a limited number of studies have utilised a mixture, chiefly as a means to reduce the vaporisation threshold and provide a more varied composition for different applications. Mixed PFC cores could be further developed to continue broader evaluations of nanodroplets properties (Zhang W. et al., 2022).

### 1.1.3 Importance of shell and core composition

PCNDs are controllable, on-and-off contrast agents that can be vaporized (i.e., activated) and destroyed or recondensed (i.e., deactivated) by control of activation parameters and the properties of nanodroplets including the volatility of the PFC core, shell material and size distribution (Burgess et al., 2022; Van Namen et al., 2021). The PCNDs can recondense back to a liquid state and undergo the expansion-recondensation cycle or can remain as gas MBs and be cleared from the body within minutes to hours, depending on environmental conditions, PFC core composition, differences in interfacial properties of shell, type and temperature of the liquid PCNDs suspension (Hannah et al., 2016; Yu et al., 2016; Yoo et al., 2018). For instance, agarose PCNDs suspension leads to recondensation rather than fragmentation compared with flow tube phantoms (Yoo et al., 2018). Also, PFC core composition significantly impact recondensation or dissolution into the surrounding environment. PCNDs composed of $C_6F_{14}$ and $C_5F_{12}$ cores are more likely to experience recondensation to a liquid state after insonation in comparison to $C_4F_{10}$ at 37°C (Ishijima et al., 2016; Luke et al., 2016; Welch et al., 2022). However, there is evidence of low-boiling-point PCNDs being activated and deactivated by ultrasound pulses (Zhang et al., 2018a; Riemer et al., 2022). In addition, differences in interfacial properties of the lipid shelled PCNDs affect the recondensation of the MBs. The high proportion of PEGylated lipids in the 10:90 PCNDs encourage rapid recondensation of the PCNDs due to stiffer encapsulating shells.

## 1.2 Fabrication techniques of PCNDs

There are several preparation techniques for phase-change nanodroplets, including microbubble condensation, sonication, homogenisation, extrusion, and microfluidics (de Gracia Lux et al., 2017; Sheeran et al., 2012). These different preparation techniques influence nanodroplet size and uniformity. Size is a critical parameter for the activation pressure threshold since larger droplet sizes reduce vaporisation thresholds (Sheeran et al., 2016; Gorelikov et al., 2011). Size also has an inverse relation to vaporisation thresholds. Selection of an appropriate method for preparing PCNDs is critical to improve uniform activation of nanodroplets under ultrasound energy (Lee et al., 2015) as nanodroplets with a low polydispersity will respond more uniformly under ultrasound energy (Song et al., 2016).

MBs condensation is effective for producing liquid nanodroplets from highly volatile PFC (e.g., $C_3F_8$, $C_4F_{10}$) that exist as a gas at room temperature (Gorelikov et al., 2011). In this method, MBs with a volatile PFC core are condensed under pressure and cooling into liquid state droplets (Meng et al., 2019). Transition of the core from a gas to a liquid result in the reduction in size and a submicron distribution of droplets. This relatively simple method prepares a high concentration of volatile PCNDs. In addition, particles, dyes and targeting ligands can be attached to the nanodroplet surface with relative ease (Rojas et al., 2019; Helfield et al., 2016; Rapoport, 2016). Generating droplets with a narrow size distribution is difficult since most microbubbles tend to be polydisperse (Vlaisavljevich et al., 2016). The condensation method can generate relatively small

nanodroplets, where researchers reported PCNDs with a size of 117 nm (Zhang et al., 2019a).

Sonication is a simple method for generating nanoparticles (including PCNDs) that are uniform in size and distribution. In this method, the components of droplets including shell material and PFC are combined by ultrasound in an aqueous phase or buffer solution. The vial is commonly kept in an ice bath during sonication to prevent excess heating (Apfel, 1998). A sonication bath (Singh et al., 2012) and probe sonicator (Kripfgans et al., 2000) are two types of sonication. Longer sonication time and sonication intensity result in a lower size and superior size dispersity compared to shorter times and intensities (Li et al., 2014). While this method is convenient, cost-effective, and avoids material loss compared with other techniques, low nanodroplet uniformity (Gao et al., 2008), and risk of contamination with metals during preparation (following probe tip erosion) (Stride and Coussios, 2010). The sonication method however can generate much smaller nanodroplets in comparison to most techniques, where researchers reported PCNDs with a size of 46 nm (Burgess et al., 2022).

Agitation/homogenisation methods range from shaking by hand to automated homogenisation systems (Miles et al., 2016; Strohm et al., 2012). In these methods, firstly, the shell components with an aqueous solution are mixed, then PFC is added and homogenised into emulsions. Although these techniques avoid material loss (as production of the entire droplet solution remains within a single container), they generate a wide size distribution of nanodroplets with low reproducibility (Lanza et al., 1996). Researchers reported PCNDs with sizes varying from 300 nm to micrometers (Miles et al., 2016; Strohm et al., 2012; Lanza et al., 1996).

Extrusion is often utilised in combination with other techniques including sonication and condensation. Whilst this technique is more complex than sonication approaches, extrusion methods can generates highly monodisperse solutions where researcher producing nanodroplets ranging from 250 to 400 nm (Lee et al., 2015; Sheeran et al., 2011a).

Microfluidics offers another fabrication method to produce uniform emulsions. There are two types of microfluidics for droplet preparation: passive or active. In most instances, PCNDs are generated using the passive method. In a passive microfluidic device, while a continuous phase (an aqueous phase) is injected into the first inlet cartridge, the organic phase containing PFC and shell material is injected into the second inlet via a pressure-driven flow (Couture et al., 2006). When two phases meet at a junction, the PFC liquid extends and form a droplet (Airan et al., 2017). Active techniques generate droplets with the aid of additional energy inputs such as electrical, magnetic, and/or centrifugal controls, or by changing intrinsic parameters like flow velocity and material properties to improve viscous, inertial, and capillary forces (Couture et al., 2006). Microfluidics produce monodisperse size distributions which provide highly uniform activation thresholds and improve vaporisation efficiency (Apfel, 1998). However, this technique has limited production speed and require relatively expensive and specialised equipment (Lea-Banks et al., 2019). Nanofluidic devices or a combination of both fluidic methods would bolster the technique and improve nanodroplet yields with a capability to generate nanodroplets varying from 50 to 2,500 nm (Reznik et al., 2013; Toprakcioglu et al., 2020). Melich et al. used microfluidic system parameters to generate PCNDs in the range of 200–400 nm with high uniformity, which is of paramount importance for therapeutic applications. The resulting PCNDs including surfactant and PLGA polymer PCNDs ($C_5F_{12}$, $C_6F_{14}$) showed good stability properties upon storage at 4°C over a period of 1 month without any impact on size and polydispersity (Melich et al., 2020).

### 1.3 Size distribution

The appropriate size of nanodroplets depends on the therapeutic applications including both within the vessel and beyond the vasculature. BBB opening (Chen et al., 2013), endothelial targeting (Wang et al., 2013), embolotherapy (intentional occlusion of the blood supply to tumours) (Zhang et al., 2010) are relevant to blood vessels, whilst delivery of chemotherapeutic agents (Rapoport, 2012) extends beyond the vasculature. Identification of suitable ways for tailoring the PCND size and size distribution during manufacturing is favourable because PCNDs size and size distribution have an effective influence on their behaviour *in vivo*, including extravasation efficiency, circulation time, and response to ultrasound stimulation. While increasing the volumetric concentration of PCNDs cores resulted in an increase in PCND size, increasing the time and power of sonication led to decreases in both size and size dispersity (Ferri et al., 2021; Aliabouzar et al., 2019). Approximate droplet diameters for extravasation in tumour tissue is <500 nm (Rapoport, 2012) whilst extravasation in healthy tissue is <20 nm (Baronzio et al., 2009). Importantly, as shown in canine kidneys, nanodroplets ≥3 μm may block pulmonary capillaries (Zhang et al., 2010). Thus, identifying appropriate droplet sizes that are able to pass freely along blood vessels is critically important for systemic delivery. Both experimental and computational studies have showed that droplet diameter and vaporisation thresholds are inversely proportional (Kripfgans et al., 2004; Shpak et al., 2014), whilst other studies have demonstrated that increasing volumetric PCNDs concentration leads to larger size of PCNDs (Wong et al., 2011; Kripfgans et al., 2004).

## 2 Application of PCNDs

PCNDs have several specific features including biocompatible components, phase-change dynamics, ultrasound imaging contrast agents and both therapeutic and diagnostic application (Zhang et al., 2018a; Lin et al., 2018; Qin et al., 2021a; Zhu et al., 2020). While nanodroplets are able to pass through pores of hyperpermeable vessel walls in tumours and accumulate in tumour tissue, MBs are unable to enhance image contrast outside blood vessels due to their short circulation time and large particle size (Reznik et al., 2011). In addition, PCNDs circulate longer in the bloodstream and remain at the nano-scale size, offering several advantages over MBs. Vaporization of nanodroplet cores following exposure to a sufficiently high-intensity pulse of acoustic energy enables echogenic microbubbles to be used as appropriate contrast agents for ultrasound imaging (Kripfgans et al., 2000; Loskutova et al., 2019). Environmental factors, droplet design, and ultrasound parameters affect the ultrasound pressure required for PCNDs

and are thus key aspects to control across all applications (Sheeran and Dayton, 2012).

## 2.1 Ultrasound imaging

Ultrasound imaging can be done in real-time, at a high framerate, and without the need for ionising radiation. Compared to other imaging modalities, it is relatively low cost and portable (Hannah et al., 2014) (Wu et al., 2011). The phase transition of nanodroplets (liquid-gas transition) by ultrasound waves generates acoustic emissions, which can be visualised via a B-mode imaging, contrast enhanced ultrasound imaging, or super-resolution ultrasound imaging methods (Kripfgans et al., 2000; Wu et al., 2021; Baghbani et al., 2017; Simpson et al., 1999; Zhang G. et al., 2022). This acoustic imaging helps to monitor the size of MBs through harmonic emissions generated by vaporised nanodroplets (Gao et al., 2008; Harput et al., 2019). Although the nano-scale size of nanodroplets results in longer circulation times and better *in vivo* stability, they are undetectable by conventional ultrasound imaging before vaporisation (Mannaris et al., 2019). Controllable activation and stable oscillation of nanodroplets is therefore critical to generate high-contrast images (Yoon, 2021; Zhang et al., 2019b), therefore it is crucial to control and tune the ultrasound parameters to avoid MB destruction.

Researchers used PCNDs with all four PFC cores as an ultrasound contrast agent for imaging. Namen et al. utilized high-intensity focused ultrasound (HIFU) pulses to achieve ADV for PCNDs with $C_5F_{12}$ and $C_6F_{14}$ cores at 1.1 MHz with an MI of 7.6. They demonstrated that repeated acoustic activation of PCNDs with $C_6F_{14}$ core can be achieved using shorter-duration (1–100 cycles) pulses that allow nanodroplet vaporization and recondensation. They also showed that longer-duration (10,000 cycles) pulses are not suitable for contrast-enhanced ultrasound imaging as they destroy the activated nanodroplets (Van Namen et al., 2021). Dayton et al. showed that PCNDs with a mixed $C_5F_{12}$ and $C_6F_{14}$ core can be used for targeted imaging on a cell monolayer by using acoustic radiation force to push them towards the cells without activating them (Dayton et al., 2006). Puett et al. investigated the different pulse sequences for activation of PCNDs with $C_3F_8$ and $C_4F_{10}$ cores. They used single-cycle pulses at 9 MHz for imaging before and after activation of PCNDs and focused pulses at 5 MHz using 32, 64, 96, or 128 elements transducer which included 2, 5, 10, or 15 cycles per pulse for activation of $C_3F_8$ and $C_4F_{10}$. The size of the MBs cloud in the images increased steadily as a function of the number of cycles for $C_4F_{10}$ from 2.5 to 4.4 $mm^2$, while averaging 8 $mm^2$ MB clouds were observed for $C_3F_8$ (Puett et al., 2014). Ge et al. provided fast acoustic wave sparsely activated localization microscopy to simultaneously image, activate and deactivate low boiling point $C_3F_8$ using high frame rate planewave ultrasound without the need of using focus-wave transmission waves. This technique provides ultrasound super-resolution images in milliseconds which overcomes main challenge of ultrasound super-resolution imaging using MBs including the long acquisition time together with the motion during the data acquisition (Zhang et al., 2018b) (Zhang G. et al., 2023).

## 2.2 Targeted drug delivery

Delivery of therapeutic agents to different parts of body is an essential part of successful treatment (Cao et al., 2018). Previously, MBs were utilised as drug carriers for local release in combination with ultrasound, which were considered a novel and reliable tool for image-mediated tumour targeting, therapy, and monitoring (Lea-Banks and Hynynen, 2021; Kopechek et al., 2015; Mozafari et al., 2016). Although this technique has strong potential for future clinical applications, MBs as drug carriers are marred by several inherent problems. Firstly, although tumour tissue has defective vasculature with much bigger endothelial capillary gaps (380–780 nm) compared to normal tissues, the micro-sized MBs are not able to extravasate into tumour tissue (SK et al., 1998). Thus, limitation of direct targeting of MBs to tumour narrows down molecular ultrasound modality to intravascular imaging and therapy (Wilson et al., 2013; Pysz et al., 2015). Moreover, the short circulation time of MBs (half-life of 3–15 min) hinders tumour-specific drug release and application of MB-based ultrasound molecular imaging and therapy (Liu et al., 2017).

PCNDs as nano-sized drug carriers are able to passively extravasate into tumour tissue through gap junctions between vascular endothelial cells due to the immature morphological characteristics of tumour vessels, improving intertumoral drug accumulation by the enhanced permeability and retention (EPR) effect (Rapoport et al., 2013; Sheeran et al., 2011a; Zhao et al., 2023; Rapoport et al., 2009; Maghsoudinia et al., 2022; Song et al., 2021; Xu et al., 2016; Ho et al., 2016). One study by Spatarelu et al. demonstrated drug loaded $C_5F_{12}$ nanodroplets for treatment of breast cancer in mouse models. Following the mice tail vein injections of the 100 μL of drug loaded nanodroplets, a series of ultrasound pulses (515 kHz, 5.7 MPa peak focal pressure, 10 cycles) were transmitted to activate nanodroplets, which resulted in expulsion of the loaded drugs in the targeted area. Results indicated that activation of nanodroplets enhances the drug-delivery effect and delays the tumour growth rate *in vivo* (Spatarelu et al., 2023).

## 2.3 Blood brain barrier (BBB) opening

BBB is the leading biological barrier which highly prevents effective therapeutic agents from entering into brain parenchyma and functioning properly. Different therapeutic agents include chemotherapeutic molecules (Park et al., 2012), neurotrophic factors (Baseri et al., 2012), antibodies (Jordão et al., 2010), siRNA (Burgess et al., 2012), and neural stem cells (Burgess et al., 2011). These therapeutic agents are able to pass through BBB and have been shown to elicit therapeutic effects (Chen et al., 2013). In addition, higher doses of drugs are needed to enter brain for an effective therapeutic concentration at diseased tissues due to obstruction from the BBB. (Wu et al., 2018; Zhang X. et al., 2017). Focused ultrasound (FUS) increases the transcellular and paracellular permeability of BBB in the presence of MBs (Chen et al., 2013; Zhang X. et al., 2017). The response of MBs to ultrasound (Liu et al., 2014)including repetitive contraction and expansion (oscillations or stable cavitation) and collapse (inertial cavitation and generation of forceful shock waves and microjets)

(Giesecke and Hynynen, 2003; Liu et al., 2014), can break tight junctions between the brain endothelial cells and create pores within the cell membrane (Husseini et al., 2005) that increases BBB permeability. However, because of the comparatively larger size of MBs (>1 μm) and short circulation half-life, extravasation into the brain is challenging (Sirsi et al., 2010). Thus, BBB opening present a unique challenge compared to targeted drug delivery to other parts of body. Therefore, PCNDs, which have a smaller size and longer circulation half-life for FUS induced BBB opening than MBs were utilised. BBB opening is caused not only by vaporization of nanodroplets, but also oscillations of generated MBs, therefore it is crucial to control and tune the ultrasound parameters to avoid MB destruction.

Chen et al. compared the effect of acoustically-activated nanodroplets on targeted drug delivery in the brain after FUS-induced BBB opening in mice. Fluorescently labelled dextran as a model drug molecule was utilized to quantify the extent of BBB opening. Comparison between PCNDs and the conventional contrast agent, i.e., MBs with similar lipid composition was conducted. Analysis of the acoustic emission generated from the contrast agents during sonication gave insights to the characteristics of PCNDs and MBs (Xu et al., 2020). A linear correlation between BBB permeabilization and the acoustic emission was found for both PCNDs ($R^2$ = 0.74) and MBs ($R^2$ = 0.67) by passive cavitation detection. PCNDs-mediated dextran delivery to the targeted murine hippocampus was achieved using sonication pressures higher than 0.45 MPa at clinically relevant pressure amplitudes. Although PCNDs had a higher BBB opening pressure threshold, they had lower stable cavitation threshold than the MBs. A more homogeneous dextran delivery within the targeted hippocampus without inducing inertial cavitation (IC) or compromising safety was achieved using PCNDs (Chen et al., 2013).

Zhang et al. utilized continuous FUS sonication for three or 5 min at 1.0 MPa after intravenous administration of $C_5F_{12}$ nanodroplets with poly (ethyleneglycol) - poly (lactide-co-glycolic acid) shells (10 mg/kg) into the rats 'tail vein. Quantitative and qualitative analysis of Evan's Blue extravasation in the right cerebral hemisphere (treatment side) of rat brains showed a greater area of BBB opening via FUS combined with nanodroplets compared to the contralateral control (Zhang X. et al., 2017).

## 2.4 Sonothrombolysis

Sonothrombolysis is a minimally invasive, ultrasound-facilitated blood clot ablating technique (Chuang et al., 2012). This technique is utilised for treatment of thrombo-occlusive vascular disease, including pulmonary embolism and deep vein thrombosis (Presset et al., 2020). Acoustic cavitation including stable and inertial cavitation (IC) is one of the mechanisms of sonothrombolysis (Fix et al., 2017; Wright et al., 2011; Datta et al., 2006). Generated force and shear stress by MBs contrast agents (used as cavitation nuclei) result in clot dissolution (Prokop et al., 2007; Kim et al., 2017). MBs oscillate and burst near the clot with lower peak negative pressure (PNP) amplitude (0.5–2 MPa) than the free-bubble nucleation threshold (PNP > 13.5 MPa) (Prokop et al., 2007; Kim et al., 2017; Acconcia et al., 2014). However, MBs-based sonothrombolysis is time-consuming, requiring hours for clot dissolution and is therefore not appropriate for aged and retracted clots (Zhang et al., 2016; Sutton et al., 2013) due to large size of microbubbles which start cavitation-enhanced erosion of blood clots from the external clot surface (Collis et al., 2010).

Therefore, PCNDs were utilised for sonothrombolysis due to their smaller size, resulting in more effective permeation into each clot and enhancement of sonothrombolysis. Kim et al. compared thrombolytic effects of lipid-shell $C_4F_{10}$ nanodroplets with those of MBs with the same formulation, in an aged bovine blood clot flow model. Ultrasound pulsing schemes with 0.35 and 5.22 W/cm$^2$ power using PCNDs generated a significant difference ($p < 0.05$) in nanodroplet-mediated sonothrombolysis performance compared with MBs with the same formulation. Nanodroplet-mediated sonothrombolysis treatment reached a 140% average thrombolysis rate over the MBs-mediated treatment. While nanodroplet-mediated ultrasound treatment created internal erosion in the middle of bovine clot samples and cavitation clouds throughout each clot, MBs-mediated ultrasound treatment created larger cavitation clouds only at the clot surface (Kim et al., 2020).

## 2.5 Histotripsy

Thermal ablation is the application of external energy to a tissue to induce irreversible cell injury, tissue necrosis and tumour destruction (Kripfgans et al., 2014; Phillips L. C. et al., 2013; Chu and Dupuy, 2014). These heat-based techniques are divided into the heat-based modalities including radiofrequency (RF), microwave (MW), HIFU (Moyer et al., 2015; Pajek et al., 2014; Chang et al., 2018; Puett et al., 2013), and laser ablation (Zhang Q. et al., 2023; Zhang et al., 2019c; Thermal ablation, 2011; Hannah et al., 2016). HIFU is the only non-invasive hyperthermic modality which utilizes and focuses multiple ultrasound beams on a selected focal area to generate temperatures of up to 60°C, in turn causing acoustic cavitation and coagulative necrosis (Haen et al., 2011). In acoustic cavitation, acoustic pressure causes expansion and contraction of gaseous nuclei in cells, leading to the collapse of the cell and nuclear membranes (Haen et al., 2011). However, HIFU utilizes continuous or long bursts of ultrasound at moderately high intensity and high duty cycle to heat tissue which is used infrequently in the clinic (Xu et al., 2021). Histotripsy utilizes short ultrasound bursts (microseconds in length) with a low duty cycle (≤1%) to minimize heating, and higher peak negative pressure amplitudes to generate acoustic cavitation from gaseous nuclei in tissues (Khokhlova et al., 2015). Combination of histotripsy with nanodroplets results in disruption of cells similar to the sole histotripsy process but at a lower acoustic pressure (Vlaisavljevich et al., 2015a). This reduced cavitation threshold allows selective delivery of histotripsy to the tumour tissue which greatly increases the treatment efficiency. Research showed that 204 nm polymer-shell $C_5F_{12}$ nanodroplet-embedded agarose tissue phantoms containing a sheet of red blood cells needed lower peak negative pressure of 10.8 MPa for generation of MBs compared with 28.8 MPa observed using ultrasound pulses for histotripsy alone. Therefore, PCNDs-mediated histotripsy creates consistent fractionation similar to that of histotripsy alone but at a

significantly lower pressure (Glickstein et al., 2022; Vlaisavljevich et al., 2013).

# 3 Methodology

The meta-analysis was performed to provide a guideline for ADV, which means converting a liquid droplet into a gaseous microbubble by ultrasound in this case. The magnitude of ultrasound pressure needed for this phase transition is defined as the vaporisation threshold (Vlaisavljevich et al., 2015b; Vlaisavljevich et al., 2015c). However, this threshold is not only a function of the ultrasound pressure, but affected by other ultrasound transmit parameters, such as the ultrasound frequency and pulse duration, and nanodroplet characteristics, such as core composition and size. To perform the meta-analysis, search term of *"nanodroplets"* + *"ultrasound"* is used for the search. In August 2024, over 7,500 publications related to search terms have been found, where more than half of these articles are published within the last 4 years.

Within these publications, 139 articles used ultrasound to vaporise nanodroplets while clearly mentioning the ultrasound pressure, ultrasound frequency, ultrasound pulse length and the nanodroplet size. From these articles, only articles that met the following criteria were chosen to extract data for the meta-analysis:

- when exact activation parameters are mentioned, including ultrasound frequency, peak negative pressure (or mechanical index), transmit pulse length or duration.
- when size of droplets is in the nanometre range (<1 μm).
- when *in vivo* or *in vitro* experiments are performed at a temperature of 37°C.
- when the publication clearly mentioned vaporisation, phase-change or ADV of nanodroplets and the observations are not due to IC.

Articles which do not meet the above-mentioned criteria were excluded and 74 data points from 45 publications were used for the meta-analysis. (Riemer et al., 2022; Paproski et al., 2014; Burgess et al., 2022; Ho and Yeh, 2017; Sheeran et al., 2013a; Vlaisavljevich et al., 2013; Fix et al., 2017; Van Namen et al., 2021; de Gracia Lux et al., 2017; Gao et al., 2008; Sheeran et al., 2011a; Reznik et al., 2013; Chen et al., 2013; Ferri et al., 2021; Zhang et al., 2016; Lin et al., 2017a; Lin et al., 2017b; Lin et al., 2017b; Zhang et al., 2017b); Lin et al., 2016; Toulemonde et al., 2018; Deng et al., 2020; An et al., 2022)

## 3.1 ADV measurement methods

The limitations of ADV measurements and the variation between different ADV measurements are two important factors that can affect the reported ADV threshold values. Parameters influencing the ADV threshold of PCNDs include ultrasound activation parameters (frequency, peak negative pressure, transmit pulse length or duration), PCNDs characteristics (core and shell composition, size and concentration) and environmental parameters (temperature, viscosity of the surrounding fluid and boundary conditions (Sheeran et al., 2011b; Wu et al., 2021). In constrained environments, the vaporisation threshold of PCNDs increases, where it is shown that ADV pressure threshold is inversely proportional to tube size and surrounding viscosity in constrained environments (Rojas et al., 2019). This illustrates the importance of experimental design, timing and choice of activation parameters for ADV threshold. Also, the definition of the threshold is likely to vary according to the direct and indirect ADV threshold measurement methods.

Direct measurements of ADV thresholds include high-magnification microscopy and high-speed imaging providing direct observation of the vaporisation process by counting of bubbles before and after of ultrasound exposure (Kripfgans et al., 2000; Vlaisavljevich et al., 2016; Sheeran et al., 2013b). However, optical observations are not applicable to tissue and not proper for initial size measurement of PCNDs below 800 nm due to limitation of resolution in brightfield imaging (Wu et al., 2021). Indirect measurement techniques including ultrasound imaging (Porter and Zhang, 2008) and broadband emissions (Aliabouzar et al., 2018; Vlaisavljevich et al., 2015a) address abovementioned limitations to identify ADV thresholds. There is smaller field of view in an optical observation than that of an ultrasound transducer which there are fewer PCNDs and bubbles, resulting in a higher measured threshold by optical experiment compared to acoustic methods (Wu et al., 2021). Two parameters of system including sensitivity and spatial resolution have effect on the pressure threshold which is the pressure at which first detection of a gas bubble or its emission is recorded (Wu et al., 2021). The measured pressure threshold is dependent on the selected signal amplitude for ADV or IC by the researcher and other parameters such as durability of the applied coating and presence of other bubbles and their collapse.

Finally, signal processing or data processing can play an important role on the reported ADV threshold values. Wu et al. utilised the mean echo amplitude in a fixed region of interest to calculate ADV threshold from the B-mode images. The difference between five separate images for each set of exposure conditions were used to calculate an average echo amplitude. They defined the ADV threshold as the point at which the normalized relative echo amplitude was over 80% (Wu et al., 2021). Williams et al. calculated the average power of the echo envelopes within each region of interest B-mode images. They defined the ADV threshold as the point at which echo power increased above background by a factor of 5 standard deviations (Williams et al., 2013). Since researchers utilised different methods for estimating the ADV threshold value, observing variations between different studies with similar experimental conditions are inevitable.

# 4 Results

Researchers chose a wide range of ultrasound frequencies to activate PCNDs with four common PFC cores ($C_3F_8$, $C_4F_{10}$, $C_5F_{12}$ and $C_6F_{14}$) with values varying between 0.06–16 MHz. The therapeutic applications generally used a lower frequency range below 5 MHz for activating PCNDs, while imaging applications covered the whole clinical ultrasound imaging range of 1–15 MHz. Within this frequency range, the PNP changed between

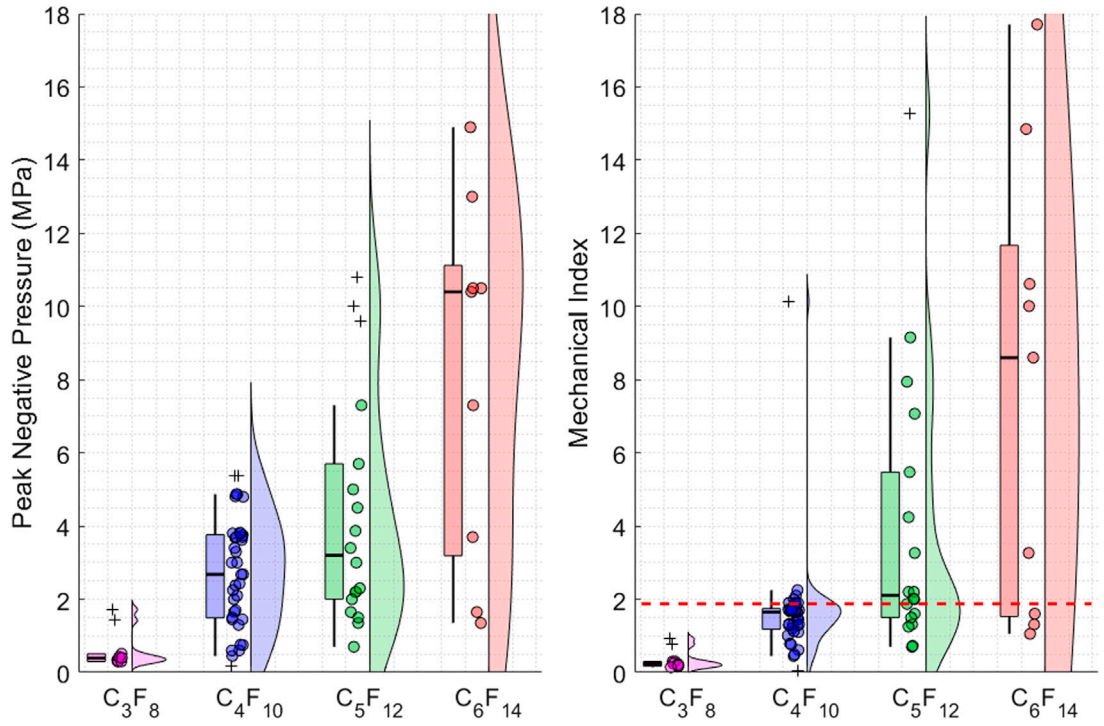


FIGURE 1
Figure illustrates the different data points, and their distributions used in the meta-analysis. Each data point plotted as a circle represents the ADV threshold for different PCNDs. The distribution of the data points is visualised as violin and box plots while converting the outlier data points from circles to crosses. (Left) Illustrates the peak negative pressure threshold values to achieve ADV and their distributions (Right) Illustrates the mechanical index threshold values to achieve ADV and their distributions. The red dashed line shows the clinical ultrasound imaging MI limit of 1.9.

0.18–14.9 MPa with excitation pulses varying from sub-microseconds to hundreds of milliseconds (0.11 μs and 640 ms). In terms of PCND parameters, the nanodroplet sizes varied between 46–595 nm for all PFC cores. The PCND concentration ranged from $10^4$ PCNDs/mL to $10^{14}$ PCNDs/mL, while most of articles (79.1%) preferred a concentration between $10^6$–$10^{10}$ PCNDs/mL. In terms of shell composition, 37 out of 45 the articles included used lipid shell, five out of 45 the articles included used polymer shell, two out of 45 the articles included used albumin shell and one out of 45 the articles included used surfactant shell.

In addition to pressure, the Mechanical Index values were calculated using the ultrasound frequency and PNP and plotted in Figure 1. This figure shows that the PCNDs with longer carbon chains require larger PNP or larger MI in general. In addition to this trend observed in Figure 1, our statistical analysis showed significant differences for ADV thresholds between all four PFCs groups ($p$-value <0.05 using two-way ANOVA method). This is expected since PFCs with longer carbon chains have higher boiling points. Figure 1(right) shows that all PCNDs with $C_3F_8$ core (8 of eight data points, 100%), most of the PCNDs with $C_4F_{10}$ core (31 out of 37 data points 83.7%), approximately half of the PCNDs with $C_5F_{12}$ core (7 out of 18 data points, 38.8%) and some of the PCNDs with $C_6F_{14}$ core (3 out of nine data points, 33.3%) can be activated within the clinical ultrasound imaging limit.

Although Figure 1 shows a trend between activation pressure and PCND core composition, it does not clearly demonstrate the relation between ultrasound activation parameters. To demonstrate the combined effects of activation parameters on ADV, a set of figures are generated. First, the ultrasound frequency and pressure relationship, which is commonly plotted by other researchers as well, is plotted in Figure 2 for all PFC cores.

Figure 2 illustrates that peak negative pressure increase with increasing frequency for PCNDs with $C_4F_{10}$ core while this trend is not clearly obvious for other cores. The reason for this can be due to the lack of data points for other PFC cores, since half of the data points in this figure are PCNDs with $C_4F_{10}$ core, which are most widely studied by researchers for ultrasound applications. There are contradicting examples in the literature, as increase in sonication frequency has been found to both increase and reduce the vaporisation threshold (Schad and Hynynen, 2010; Williams et al., 2013). Williams et al. demonstrated that a frequency increase from 5 MHz to 15 MHz decreased vaporisation thresholds of 220 nm surfactant-coated $C_5F_{12}$ nanodroplets (Williams et al., 2013). Vaporisation thresholds reduced from 6 MPa at 37°C for a 1 ms excitation at 10 MHz to 3.2 ± 0.5 MPa at 37°C for a 1 ms excitation at 15 MHz. They found that the vaporisation thresholds differed inversely with frequency at 29°C and 37°C. This inverse trend between frequency and vaporisation thresholds was also observed by Schad et al. (Schad and Hynynen, 2010) while (Kripfgans et al., 2004) for micron sized droplets, where increase in the vaporisation pressure from four to 7 MPa with increased frequency from three to 4 MHz with single 3.25 μs tone burst for albumin-coated micro-scale $C_5F_{12}$ droplets. This trend

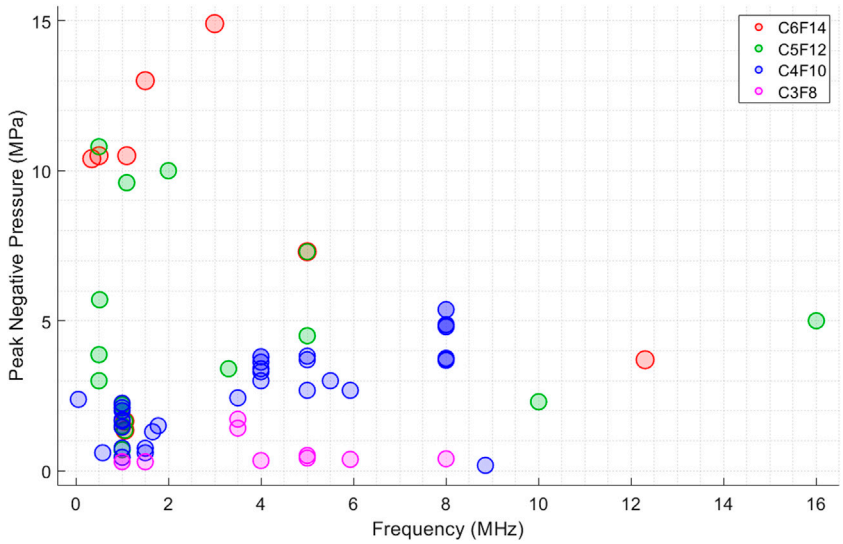


FIGURE 2
Figure shows the reported peak negative pressure (MPa) threshold values from different studies to achieve ADV at different ultrasound frequencies. Each PCNDs is illustrated in different colour. Every datapoint is plotted as transparent circles to clearly show the overlaps between datapoints.

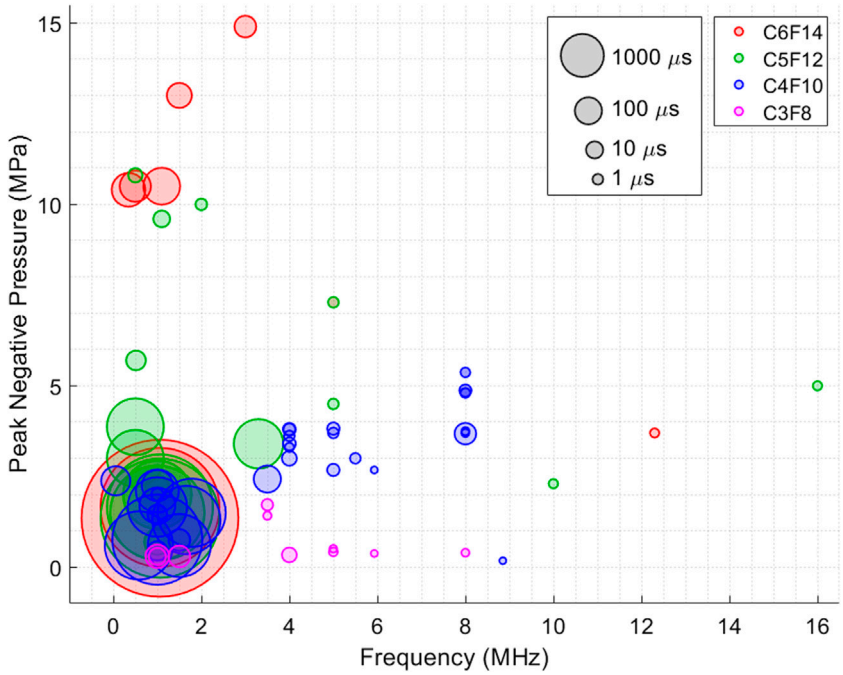


FIGURE 3
Figure shows the reported peak negative pressure (MPa) threshold values at different frequencies to achieve ADV as a function of excitation duration or pulse length. Each PCNDs is illustrated in different colour. Every datapoint is plotted as transparent circles to clearly show the overlaps between datapoints. Size of every datapoint represents ultrasound excitation duration.

may suggest a mechanical mechanism whereby activation of nanodroplets occurs through a focused spot of negative pressure inside the droplet (which spreads through its whole volume), ultimately resulting in IC (Shpak et al., 2014). However, these studies (Schad and Hynynen, 2010) used droplets larger than 1 μm and there is no evidence for an inverse relation between negative pressure and frequency for nanodroplets.

Figure 2 does not however directly represent the relation between ultrasound activation parameters and how much input energy is required for activation of PCNDs, as many other

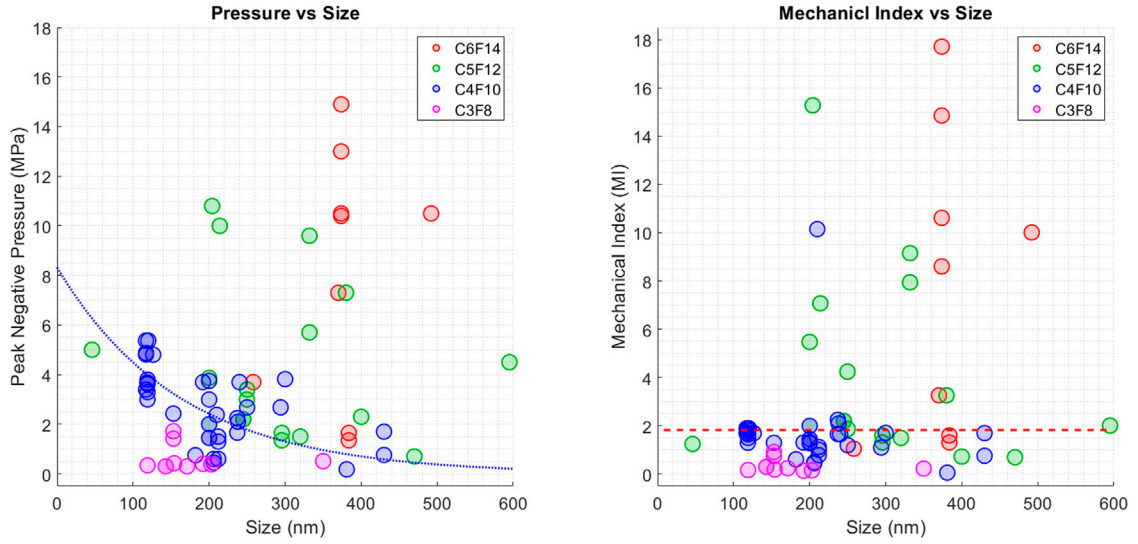


FIGURE 4
(Left) Figure shows the reported peak negative pressure (MPa) threshold values from different studies to achieve ADV for different PCND sizes. Blue dotted line illustrates the expected ADV threshold behaviour for PCNDs with $C_4F_{10}$ core (Right) Figure shows the reported Mechanical Index values from different studies to achieve ADV for different PCND sizes. The red dashed line shows the clinical ultrasound imaging MI limit of 1.9.

parameters also contribute to PCNDs activation. These parameters include environmental variables (temperature, viscosity of the surrounding fluid conditions, hydrostatic pressure, boundary constraints), nanodroplet characteristics (core and shell composition, thickness of shell, size, and concentration), and the ultrasound exposure parameters (frequency, pressure, exposure duration and pulse repetition frequency). Therefore, ADV threshold of PCNDs were plotted for different 4 PFC cores in Figure 3 by combining ultrasound frequency (MHz), peak negative pressure (MPa) and activation pulse length in a single figure to demonstrate the effect of ultrasound parameters.

Figure 3 is consistent with the studies (Wu et al., 2021; Fabiilli et al., 2009), wider circles (longer pulse length) are mostly located at lower pressures levels. Overall, the vaporisation threshold decreases with increasing droplet diameter and increasing burst length (Sheeran et al., 2011b). Additionally, the larger circles of the same PFC cores appear closer to the origin, indicating that longer pulse lengths were used at lower frequency ranges to reduce the ADV threshold. This may also explain some of the extreme cases observed in Figures 1, 2, such as the PCNDs with $C_6F_{14}$ core activated at the same pressure level with most $C_4F_{10}$ cores. According to Figure 3, longer ultrasound pulse length lowers PNP due to the inverse relationship between pulse length and pressure threshold. For example, the largest red circles appearing at much lower PNP level than smaller red circles demonstrates that pressure threshold for ADV was reduced since more energy was deployed to vaporise these $C_6F_{14}$ nanodroplets. In general, $C_6F_{14}$ and $C_5F_{12}$ cores are commonly used for therapeutic applications, while $C_4F_{10}$ and $C_3F_8$ cores often utilised for imaging applications because of their lower boiling points and hence lower ADV threshold. This might be the reason why, studies using PCNDs with $C_6F_{14}$ and $C_5F_{12}$ cores used longer duration pulses more often, where the median ultrasound pulse lengths recorded for the meta-analysis are 0.9, 2.5, 50 and 200 μs for PCNDs with $C_3F_8$, $C_4F_{10}$, $C_5F_{12}$ and $C_6F_{14}$ cores, respectively.

Although there seems to be a trend in Figure 3, a direct comparison between different PCNDs is challenging due to the number of articles referring directly to activation threshold of nanodroplets with longer carbon chains are limited. As $C_6F_{14}$ cores are commonly used for therapeutic applications and are considered as nucleation points, where activation threshold of $C_6F_{14}$ is not directly mentioned in many articles while referring to cavitation threshold instead. Schad et al. found that as the sonication frequency diminishes, the separation between ADV and IC thresholds narrows, which is likely another reason for the lack of direct information on vaporization thresholds (Schad and Hynynen, 2010).

Another parameter that plays an important role in ADV is the size of the PCNDs. Figure 4 shows the reported ADV threshold for different PCND sizes for all PFC cores. Researchers manufactured PCNDs with $C_5F_{10}$ core with a wider distribution ranging from 46 to 595 nm. The reported median nanodroplet size is smaller for PCNDs with $C_3F_8$ and $C_4F_{10}$ cores (153.5 and 200 nm) in comparison to PCNDs with $C_5F_{10}$ and $C_6F_{12}$ cores (272.8 and 373.7 nm), which might be due to the manufacturing at room temperature, where $C_3F_8$ and $C_4F_{10}$ are in gaseous form and $C_5F_{10}$ and $C_6F_{12}$ are in liquid form. According to previous studies, there is an inverse relationship between size of nanodroplets and activation pressure (Lea-Banks et al., 2019). A decreasing trend in pressure with increasing size of $C_4F_{10}$ core can also be observed in Figure 4 (left), where the blue dashed line shows the logarithmic fit to demonstrate the overall behaviour. However, this trend disappears in Figure 4 (right), where the activation of small and large PCNDs can be observed at similar MI values. This figure also provides evidence that PCNDs with all four PFC cores may be activated within the clinical ultrasound imaging MI limit of 1.9, but

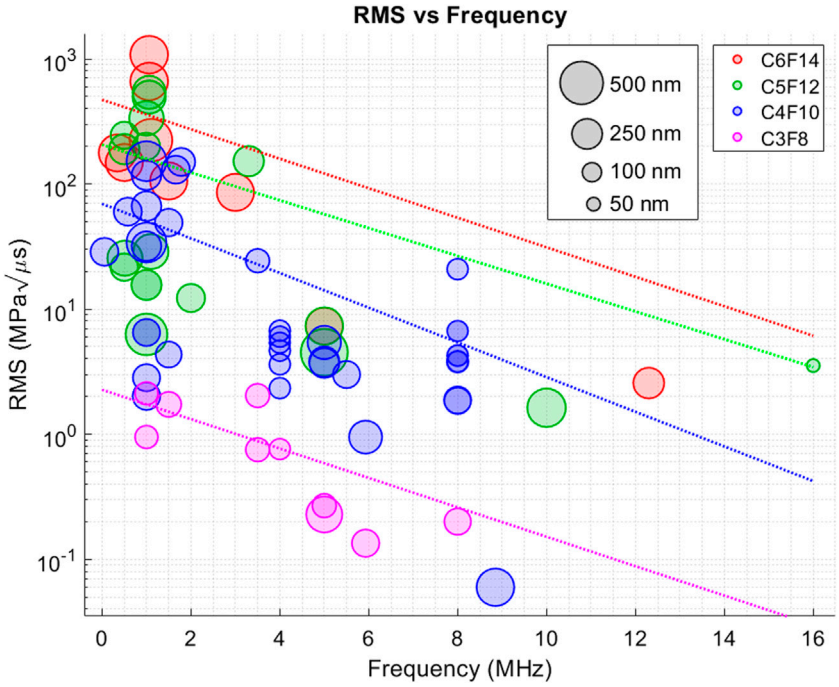


FIGURE 5
Figure shows the calculated RMS-like ADV threshold values for different ultrasound frequencies. The RMS-like power calculation was performed by combining peak negative pressure and square root of ultrasound pulse length. Each PCNDs is illustrated in different colour. Every datapoint is plotted as transparent circles to clearly show the overlaps between datapoints. Size of every datapoint represents the PCNDs diameter.

it might not be practical for many applications since PCNDs with $C_6F_{12}$ core was activated using a pulse duration over tens of milliseconds, as shown in Figure 3.

Figures 1–4 do not definitively represent or visualize the behaviour of ADV threshold because there are at least one or two missing parameters in each figure. For example, Figure 2 does not include ultrasound pulse length and nanodroplet size and Figure 3 does not include nanodroplet size. To address this, we attempted to combine and visualize all parameters at once while aiming to provide a better overall understanding and estimation of ADV threshold behaviour. Based on the inverse relationship between ADV pressure threshold and ultrasound pulse length (Pressure$^2$ $\propto$ 1/pulse length), we back-calculated this relationship by merging two parameters. This Pressure$^2$ $\propto$ 1/pulse length model was suggested Schad et al. (Schad and Hynynen, 2010) based on observations on $C_5F_{12}$ droplets at three different temperatures (23, 29°C and 37°C) over a wide range of ultrasound pulse lengths between 1 μs and 9.6 ms (Schad and Hynynen, 2010; Zhang and Porter, 2010) (Kripfgans et al., 2004). This Pressure$^2$ $\propto$ 1/pulse length relation is also consistent with the study performed by Williams et al. at 29°C (Williams et al., 2013).

To combine ultrasound PNP and pulse length, a Root Mean Square (RMS)-like metric is proposed and plotted in Figure 5 for different ultrasound frequencies. The RMS-like metric is calculated by multiplying peak negative pressure and square root of ultrasound pulse length (PNP × $\sqrt{}$ ultrasound pulse length). Note that this is not the same as RMS, since it is not possible to calculate the exact RMS power without having access to transmitted waveforms, but it is possible to get an approximation by doing this.

Figure 5 combines four parameters that play an important role on ADV threshold: ultrasound pressure, ultrasound frequency, ultrasound pulse length and the nanodroplet size. Figure 5 reveals that the RMS-like metric and ultrasound frequency might have an inverse relationship. This can be observed for PCNDs with all PFC cores. This means that that PFC nanodroplet activation require less power at higher frequencies. These results are different from our initial observations from Figure 2, where it seems as PNP threshold to achieve ADV increases with increasing ultrasound frequency. However, this observation was done only for PCNDs with $C_4F_{10}$ core and other PCNDs did not show such a behaviour. In this case, all PCNDs with different PFC cores exhibit a decreasing trend in RMS power with increasing ultrasound frequency.

## 5 Discussion

Although the relationship between activation parameters were evaluated and plotted to show the trend between parameters, a direct comparison between the studies used in this meta-analysis is challenging due to the close interaction between nanodroplet composition, size, concentration, ultrasound parameters and other experimental conditions. Nonetheless, the data gathered from several research articles agree with the figures provided in this meta-analysis. Investigation of the effect of Laplace pressure on the ADV threshold of different larger PCNDs (1–13 μm) showed that the vaporisation threshold of $C_4F_{10}$ was lower than those of the higher-boiling point PCNDs (Sheeran et al., 2011b), which is consistent with our observations from Figure 1. Two studies

showed that the ADV peak negative pressure threshold for $C_4F_{10}$ PCNDs increased with increasing ultrasound frequency (Sheeran et al., 2013b) which is consistent with Figure 2 for $C_4F_{10}$ cores. Ultrasound pulse length, or excitation duration, is another parameter which has an inverse relationship with ADV and IC thresholds. Wu et al. demonstrated that increasing the pulse length from 20 to 20,000 μs at 1 MHz reduced the ADV and IC thresholds of PCNDs with $C_4F_{10}$ core from 3.06 MPa to 2.08 MPa and from 3.36 MPa to 2.30 MPa, respectively (Wu et al., 2021). Lo et al. demonstrated similar results for PCNDs with $C_5F_{12}$ core, where the ADV threshold decreased from 5.5–5.9 MPa to 3.8–4.6 MPa, when the ultrasound pulse length is increased from microseconds to milliseconds (Lo et al., 2007). Figure 3 illustrates that longer pulse length (bigger circles) incline toward lower ADV thresholds, which is consistent with these studies. Sheeran et al. showed that the ADV peak negative pressure threshold of $C_4F_{10}$ decreased with increasing nanodroplet size (Sheeran et al., 2011b), which is consistent with our observations from Figure 4. The inverse relationship of ADV threshold to PCNDs diameter and ultrasound pulse length for $C_4F_{10}$ core has been illustrated in Figures 3, 4, which confirms that increasing PCNDs size and pulse length decreases the vaporisation threshold. The monotonic decreasing trend between vaporisation pressure and size shown in Figure 4(left) is also similar to model proposed by Sheeran et al. to describe the vaporisation pressure that has a logarithmic relation with PCND size (Sheeran et al., 2011a).

Post-vaporisation events are also crucial for choosing the most suitable nanodroplet composition and ultrasound parameters for a given application. Within activation of PCNDs, whilst some of the generated MBs survive immediately after ADV, some recondense back into the liquid droplet state within microseconds after activation. The probability of MBs survival within the first microseconds of vaporisation depends on parameters including ultrasound excitation pressure, shell material and bubble coalescence during vaporisation. While small bubbles have a higher recondensation probability due to an increase in Laplace pressure (Kabalnov et al., 1998), bigger bubbles above the radius of approximately R = 1 μm have lower Laplace pressure and this thus decreases or eliminates the possibility of a condensation or recondensation event completely (Reznik et al., 2013). In addition, microbubble size is not the only parameter affecting the probability of survival. Shell and coating material decreases the effective surface tension on the bubble and Laplace pressure (Sarkar et al., 2009; Reznik et al., 2012). Also, higher concentrations of shell material (such as surfactant coating) are more likely to prevent bubbles from condensation compared to those with less surfactant (Overvelde et al., 2010). There is higher possibility of bubble survival post-vaporisation due to more coalescence at lower excitation pressures (Haworth and Kripfgans, 2008), which would increase the total volume and size of the bubble cluster, decreasing Laplace pressure and increasing the chance of survival. The increase in size of bubbles due to coalescence of bubbles would increase surfactant coating concentration and consequently their stability. Proximity of bubbles to each other increases chance of bubble coalescence which is advantageous to increase the initial droplet concentration and to create stable MBs appropriate for ultrasound imaging. Coalescence and increasing initial droplet concentration results in a decrease in excitation pressure thresholds for the inception of stable bubbles and an increase in the probability of PFC nucleation and efficiency of production of stable bubbles (Ishijima et al., 2016). Therefore, it is important to operate close to the vaporisation threshold of PCNDs to maximise survival of MBs for imaging, as well as sonoporation and other drug delivery applications. However, the ADV threshold changes nonlinearly as a function of PCND properties, ultrasound parameters, such as peak negative pressure, frequency, pulse duration (Reznik et al., 2013) and other experimental conditions. For this reason, our meta-analysis study proposes a different way of determining the ADV threshold based on an RMS-like power measurement given in Figure 5.

This newly proposed RMS power metric may provide guidance on the effect of ultrasound frequency on ADV threshold, where this relation is not consistent across many studies. While some studies reported that the ADV threshold increases with increasing ultrasound frequency (Aliabouzar et al., 2018; Kripfgans et al., 2004; Vlaisavljevich et al., 2015b), other studies showed an opposite trend, where decreasing ultrasound frequency would increase the ADV threshold (Williams et al., 2013; Burgess et al., 2012; Kripfgans et al., 2002). This may suggest that change in the role of IC in ADV for lower frequencies, as IC threshold in the host medium approaches the ADV threshold with decreasing frequency, probably making IC be the dominant mechanism for triggering ADV (Fabiilli et al., 2009). Schad et al. found that there was no separation was found between the ADV vaporisation and IC thresholds by decreasing frequency from 2.855 to 0.578 MHz for lipid-coated $C_5F_{12}$ droplets and IC occurred instantly after sonication at the lowest pressure utilised for micron sized droplets (Schad and Hynynen, 2010). (Fabiilli et al., 2009). For micron sized droplets, researchers showed that IC threshold occurred at a higher rarefactional pressure than the ADV threshold which ADV nucleus is internal to the droplet, while IC nucleus is likely to be the bubble generated by ADV (Fabiilli et al., 2009), which is yet to be demonstrated for nanodroplets. The tailoring acoustic parameters and design and fabrication of droplets depending on the therapeutic application is important to achieve either ADV with IC or ADV without IC (Sirsi and Borden, 2009; Fabiilli et al., 2009; Chandan et al., 2020). It is suggested that the frequency at which the ADV and IC thresholds overlap may be controlled by the droplet size (Lea-Banks et al., 2019). However, IC and ADV are two overlooked phenomena in several studies. Many articles only measure and mention cavitation threshold or activation, but do not exactly mention if this is a result of ADV or IC (Qin et al., 2021b; Toulemonde et al., 2020; DeRuiter et al., 2019). The experimental measurements require a tight control on ultrasound parameters and other variables, such as temperature, PCND stability and concentration, otherwise the measurements can be dominated by the cavitation signal generated by MBs activated without droplet vaporisation.

When the ADV and IC are clearly identified, combining ultrasound peak negative pressure and pulse length, as given in Figure 5, can be useful for identifying the ADV threshold behaviour. The proposed RMS-like power metric can also benefit from including pulse repetition frequency (PRF) into these calculations. Studies report that ADV thresholds typically have an inverse relationship with PRF and pulse length, which therefore means that longer PRF and pulse length decreases the ADV threshold (Kripfgans et al., 2000; Rojas et al., 2019; Porter and

Zhang, 2008). Wu et al. investigated the effect of the PRF ranging from 1 to 100 Hz on ADV and IC thresholds for 238 nm PCNDs with $C_4F_{10}$ core whereby the frequency and pulse length were set to 1 MHz and 5,000 cycles, respectively (Wu et al., 2021). Their results showed that with increasing PRF from 2 to 100 Hz, the ADV and IC thresholds were found to decrease from 2.79 to 1.8 MPa and from 3.03 to 2.05 MPa, respectively. This is likely that increasing either the PRF or pulse length would increase the probability of ADV and the expected number of activations over the course. For our meta-(182) analysis study, many articles did not include or mention the PRF, so it was not possible to integrate this into our calculations for all data points.

## 6 Conclusion

This article outlines an overview of the effect of different ultrasound parameters on activation of PCNDs with different cores. To achieve this, a meta-analysis was conducted for a range of activation parameters, including the ultrasound frequency, peak negative pressure, ultrasound pulse length, nanodroplet core composition and nanodroplet size for experiments performed at a temperature of 37°C. A direct comparisons between data gathered from different studies is not possible due to the close interaction between nanodroplet size, concentration, ultrasound parameters, experimental setup, ambient temperature, ambient pressure and various application-dependent variables. Although each of these parameters can significantly affect ADV threshold, our findings showed that an RMS-like power metric may be an effective parameter to consider for ADV. The results presented in Figure 5 showed that less power may be required for activating PCNDs at higher ultrasound frequencies. This might be because of an increase in local temperature around the PCNDs due to the absorption of ultrasound waves within the host medium or PCND shell, where absorption increases with increasing ultrasound frequency. However, an experimental study is required to prove this phenomenon, and at this stage this is only a speculation based on our observations through previously published research articles.

## Author contributions

MD: Conceptualization, Data curation, Formal Analysis, Funding acquisition, Investigation, Methodology, Project administration, Resources, Software, Supervision, Validation, Visualization, Writing - original draft, Writing - review and editing. OH: Methodology, Writing - original draft, Writing - review and editing. HS: Formal Analysis, Methodology, Software, Visualization, Writing - original draft, Writing - review and editing. GZ: Investigation, Methodology, Writing - original draft, Writing - review and editing. MT: Funding acquisition, Resources, Supervision, Writing - original draft, Writing - review and editing, Investigation, Methodology. NG: Funding acquisition, Resources, Supervision, Writing - original draft, Writing - review and editing. GT: Funding acquisition, Resources, Supervision, Writing - original draft, Writing - review and editing. MG: Project administration, Funding acquisition, Resources, Supervision, Writing - original draft, Writing - review and editing. SH: Conceptualization, Data curation, Formal Analysis, Funding acquisition, Investigation, Methodology, Project administration, Resources, Software, Supervision, Validation, Visualization, Writing - original draft, Writing - review and editing.

## Funding

The author(s) declare that financial support was received for the research, authorship, and/or publication of this article. This work was performed as part of the project titled “Enhancing Blood-Brain Barrier Opening with Ultrasound and Microwaves for Targeted Drug Delivery”, which is supported by the MRC (MR/Z503848/1). GZ is partially supported by Natural Science Foundation of Hubei Province of China (No. 2023AFB289).

## Conflict of interest

Authors NG and GT was employed by the Umbria Bioengineering Technologies Srl.

The remaining authors declare that the research was conducted in the absence of any commercial or financial relationships that could be construed as a potential conflict of interest.

## Publisher’s note



## References

Acconcia, C., Leung, B. Y., Manjunath, A., and Goertz, D. E. (2014). Interactions between individual ultrasound-stimulated microbubbles and fibrin clots. *Ultrasound Med. Biol.* 40 (9), 2134–2150. doi:10.1016/j.ultrasmedbio.2014.03.008

Airan, R. D., Meyer, R. A., Ellens, N. P., Rhodes, K. R., Farahani, K., Pomper, M. G., et al. (2017). Noninvasive targeted transcranial neuromodulation via focused ultrasound gated drug release from nanoemulsions. *Nano Lett.* 17 (2), 652–659. doi:10.1021/acs.nanolett.6b03517

Aliabouzar, M., Kumar, K. N., and Sarkar, K. (2018). Acoustic vaporization threshold of lipid-coated perfluoropentane droplets. *J. Acoust. Soc. Am.* 143 (4), 2001–2012. doi:10.1121/1.5027817

Aliabouzar, M., Kumar, K. N., and Sarkar, K. (2019). Effects of droplet size and perfluorocarbon boiling point on the frequency dependence of acoustic vaporization threshold. *J. Acoust. Soc. Am.* 145 (2), 1105–1116. doi:10.1121/1.5091781

An, J., Zhang, J., Dong, F., Yin, J., Feng, F., Guo, W., et al. (2022). Arterial labeling ultrasound subtraction angiography (ALUSA) based on acoustic phase-change nanodroplets. *Small* 18 (12), 2105989. doi:10.1002/smll.202105989

Apfel, R. E. (1998) “No title,” in *Activatable infusable dispersions containing drops of a superheated liquid for methods of therapy and diagnosis*.

Baghbani, F., Chegeni, M., Moztarzadeh, F., Hadian-Ghazvini, S., and Raz, M. (2017). Novel ultrasound-responsive chitosan/perfluorohexane nanodroplets for image-guided

smart delivery of an anticancer agent: curcumin. *Mater. Sci. Eng. C* 74, 186–193. doi:10.1016/j.msec.2016.11.107

Baronzio, G., Fiorentini, G., and Cogle, C. R. (2009). *Cancer microenvironment and therapeutic implications*. Springer.

Baseri, B., Choi, J. J., Deffieux, T., Samiotaki, G., Tung, Y., Olumolade, O., et al. (2012). Activation of signaling pathways following localized delivery of systemically administered neurotrophic factors across the blood–brain barrier using focused ultrasound and microbubbles. *Phys. Med. and Biol.* 57 (7), N65–N81. doi:10.1088/0031-9155/57/7/n65

Borden, M. A., Shakya, G., Upadhyay, A., and Song, K. (2020). Acoustic nanodrops for biomedical applications. *Curr. Opin. colloid and interface Sci.* 50, 101383. doi:10.1016/j.cocis.2020.08.008

Burgess, A., Ayala-Grosso, C. A., Ganguly, M., Jordão, J. F., Aubert, I., and Hynynen, K. (2011). Targeted delivery of neural stem cells to the brain using MRI-guided focused ultrasound to disrupt the blood-brain barrier. *PloS one* 6 (11), e27877. doi:10.1371/journal.pone.0027877

Burgess, A., Huang, Y., Querbes, W., Sah, D. W., and Hynynen, K. (2012). Focused ultrasound for targeted delivery of siRNA and efficient knockdown of Htt expression. *J. Control. Release* 163 (2), 125–129. doi:10.1016/j.jconrel.2012.08.012

Burgess, M. T., Aliabouzar, M., Aguilar, C., Fabiilli, M. L., and Ketterling, J. A. (2022). Slow-flow ultrasound localization microscopy using recondensation of perfluoropentane nanodroplets. *Ultrasound Med. Biol.* 48 (5), 743–759. doi:10.1016/j.ultrasmedbio.2021.12.007

Canavese, G., Ancona, A., Racca, L., Canta, M., Dumontel, B., Barbaresco, F., et al. (2018). Nanoparticle-assisted ultrasound: a special focus on sonodynamic therapy against cancer. *Chem. Eng. J.* 340, 155–172. doi:10.1016/j.cej.2018.01.060

Cao, Y., Chen, Y., Yu, T., Guo, Y., Liu, F., Yao, Y., et al. (2018). Drug release from phase-changeable nanodroplets triggered by low-intensity focused ultrasound. *Theranostics* 8 (5), 1327–1339. doi:10.7150/thno.21492

Chandan, R., Mehta, S., and Banerjee, R. (2020). Ultrasound-responsive carriers for therapeutic applications. *ACS Biomaterials Sci. and Eng.* 6 (9), 4731–4747. doi:10.1021/acsbiomaterials.9b01979

Chang, N., Lu, S., Qin, D., Xu, T., Han, M., Wang, S., et al. (2018). Efficient and controllable thermal ablation induced by short-pulsed HIFU sequence assisted with perfluorohexane nanodroplets. *Ultrason. Sonochem* 45, 57–64. doi:10.1016/j.ultsonch.2018.02.033

Chen, C. C., Sheeran, P. S., Wu, S., Olumolade, O. O., Dayton, P. A., and Konofagou, E. E. (2013). Targeted drug delivery with focused ultrasound-induced blood-brain barrier opening using acoustically-activated nanodroplets. *J. Control. Release* 172 (3), 795–804. doi:10.1016/j.jconrel.2013.09.025

Chu, K. F., and Dupuy, D. E. (2014). Thermal ablation of tumours: biological mechanisms and advances in therapy. *Nat. Rev. Cancer* 14 (3), 199–208. doi:10.1038/nrc3672

Chuang, Y., Cheng, P., and Li, P. (2012). Combining radiation force with cavitation for enhanced sonothrombolysis. *IEEE Trans. Ultrason. Ferroelectr. Freq. Control* 60 (1), 97–104. doi:10.1109/tuffc.2013.2541

Collis, J., Manasseh, R., Liovic, P., Tho, P., Ooi, A., Petkovic-Duran, K., et al. (2010). Cavitation microstreaming and stress fields created by microbubbles. *Ultrasonics* 50 (2), 273–279. doi:10.1016/j.ultras.2009.10.002

Couture, O., Bevan, P. D., Cherin, E., Cheung, K., Burns, P. N., and Foster, F. S. (2006). Investigating perfluorohexane particles with high-frequency ultrasound. *Ultrasound Med. Biol.* 32 (1), 73–82. doi:10.1016/j.ultrasmedbio.2005.09.010

Datta, S., Coussios, C., McAdory, L. E., Tan, J., Porter, T., De Courten-Myers, G., et al. (2006). Correlation of cavitation with ultrasound enhancement of thrombolysis. *Ultrasound Med. Biol.* 32 (8), 1257–1267. doi:10.1016/j.ultrasmedbio.2006.04.008

Dayton, P. A., Zhao, S., Bloch, S. H., Schumann, P., Penrose, K., Matsunaga, T. O., et al. (2006). Application of ultrasound to selectively localize nanodroplets for targeted imaging and therapy. *Mol. imaging* 5 (3), 160–174. 2006. 00019. doi:10.2310/7290.2006.00019

de Gracia Lux, C., Vezeridis, A. M., Lux, J., Armstrong, A. M., Sirsi, S. R., Hoyt, K., et al. (2017). Novel method for the formation of monodisperse superheated perfluorocarbon nanodroplets as activatable ultrasound contrast agents. *RSC Adv.* 7 (77), 48561–48568. doi:10.1039/c7ra08971f

Deng, L., Lea-Banks, H., Jones, R., O'Reilly, M., An, R., and Hynynen, K. (2020). Ultrasound super resolution imaging of nanodroplets with a multi-frequency hemispherical phased array. *J. Acoust. Soc. Am.* 148 (4_Suppl. ment), 2486. doi:10.1121/1.5146889

DeRuiter, R. M., Markley, E. N., Rojas, J. D., Pinton, G. F., and Dayton, P. A. (2019). Using low-boiling point phase change contrast agent activation signals for super resolution ultrasound localization microscopy. *IEEE Int. Ultrason. Symp. (IUS)*, 1934–1936. doi:10.1109/ultsym.2019.8926020

DeRuiter, R. M., Markley, E. N., Rojas, J. D., Pinton, G. F., and Dayton, P. A. (2020). Transient acoustic vaporization signatures unique to low boiling point phase change contrast agents enable super-resolution ultrasound imaging without spatiotemporal filtering. *AIP Adv.* 10 (10), 105124. doi:10.1063/5.0029207

Fabiilli, M. L., Haworth, K. J., Fakhri, N. H., Kripfgans, O. D., Carson, P. L., and Fowlkes, J. B. (2009). The role of inertial cavitation in acoustic droplet vaporization. *IEEE Trans. Ultrason. Ferroelectr. Freq. Control* 56 (5), 1006–1017. doi:10.1109/tuffc.2009.1132

Ferri, S., Wu, Q., De Grazia, A., Polydorou, A., May, J. P., Stride, E., et al. (2021). Tailoring the size of ultrasound responsive lipid-shelled nanodroplets by varying production parameters and environmental conditions. *Ultrason. Sonochem* 73, 105482. doi:10.1016/j.ultsonch.2021.105482

Fix, S. M., Novell, A., Yun, Y., Dayton, P. A., and Arena, C. B. (2017). An evaluation of the sonoporation potential of low-boiling point phase-change ultrasound contrast agents *in vitro*. *J. Ther. ultrasound* 5, 7–11. doi:10.1186/s40349-017-0085-z

Gao, Z., Kennedy, A. M., Christensen, D. A., and Rapoport, N. Y. (2008). Drug-loaded nano/microbubbles for combining ultrasonography and targeted chemotherapy. *Ultrasonics* 48 (4), 260–270. doi:10.1016/j.ultras.2007.11.002

Giesecke, T., and Hynynen, K. (2003). Ultrasound-mediated cavitation thresholds of liquid perfluorocarbon droplets *in vitro*. *Ultrasound Med. Biol.* 29 (9), 1359–1365. doi:10.1016/s0301-5629(03)00980-3

Glickstein, B., Aronovich, R., Feng, Y., and Ilovitsh, T. (2022). Development of an ultrasound guided focused ultrasound system for 3D volumetric low energy nanodroplet-mediated histotripsy. *Sci. Rep.* 12 (1), 20664. doi:10.1038/s41598-022-25129-x

Gorelikov, I., Martin, A. L., Seo, M., and Matsuura, N. (2011). Silica-coated quantum dots for optical evaluation of perfluorocarbon droplet interactions with cells. *Langmuir* 27 (24), 15024–15033. doi:10.1021/la202679p

Haen, S. P., Pereira, P. L., Salih, H. R., Rammensee, H., and Gouttefangeas, C. (2011). More than just tumor destruction: immunomodulation by thermal ablation of cancer. *J. Immunol. Res.* 2011, 1–19. doi:10.1155/2011/160250

Hannah, A., Luke, G., Wilson, K., Homan, K., and Emelianov, S. (2014). Indocyanine green-loaded photoacoustic nanodroplets: dual contrast nanoconstructs for enhanced photoacoustic and ultrasound imaging. *ACS Nano* 8 (1), 250–259. doi:10.1021/nn403527r

Hannah, A. S., Luke, G. P., and Emelianov, S. Y. (2016). Blinking phase-change nanocapsules enable background-free ultrasound imaging. *Theranostics* 6 (11), 1866–1876. doi:10.7150/thno.14961

Harput, S., Zhang, G., Toulemonde, M., Zhu, J., Christensen-Jeffries, K., Brown, J., et al. (2019). Activation and 3D imaging of phase-change nanodroplet contrast agents with a 2D ultrasound probe. *IEEE Int. Ultrason. Symp. (IUS)*, 2275–2278. doi:10.1109/ultsym.2019.8925892

Harput, S., Zhou, X., and Tang, M. (2023) "Getting started: ultrasound physics and image formation," in *Liver ultrasound: from basics to advanced applications*, 1–22.

Haworth, K. J., and Kripfgans, O. D. (2008). Initial growth and coalescence of acoustically vaporized perfluorocarbon microdroplets. *IEEE Int. Ultrason. Symp. (IUS)*, 623–626.

Helfield, B., Black, J. J., Qin, B., Pacella, J., Chen, X., and Villanueva, F. S. (2016). Fluid viscosity affects the fragmentation and inertial cavitation threshold of lipid-encapsulated microbubbles. *Ultrasound Med. Biol.* 42 (3), 782–794. doi:10.1016/j.ultrasmedbio.2015.10.023

Ho, Y., Chang, Y., and Yeh, C. (2016). Improving nanoparticle penetration in tumors by vascular disruption with acoustic droplet vaporization. *Theranostics* 6 (3), 392–403. doi:10.7150/thno.13727

Ho, Y., and Yeh, C. (2017). Concurrent anti-vascular therapy and chemotherapy in solid tumors using drug-loaded acoustic nanodroplet vaporization. *Acta Biomater.* 49, 472–485. doi:10.1016/j.actbio.2016.11.018

Huang, Y., Vezeridis, A. M., Wang, J., Wang, Z., Thompson, M., Mattrey, R. F., et al. (2017). Polymer-stabilized perfluorobutane nanodroplets for ultrasound imaging agents. *J. Am. Chem. Soc.* 139 (1), 15–18. doi:10.1021/jacs.6b08800

Husseini, G. A., De La Rosa, M. A. D., Richardson, E. S., Christensen, D. A., and Pitt, W. G. (2005). The role of cavitation in acoustically activated drug delivery. *J. Control. Release* 107 (2), 253–261.

Ishijima, A., Tanaka, J., Azuma, T., Minamihata, K., Yamaguchi, S., Kobayashi, E., et al. (2016). The lifetime evaluation of vapourised phase-change nano-droplets. *Ultrasonics* 69, 97–105. doi:10.1016/j.ultras.2016.04.002

Izadifar, Z., Izadifar, Z., Chapman, D., and Babyn, P. (2020). An introduction to high intensity focused ultrasound: systematic review on principles, devices, and clinical applications. *J. Clin. Med.* 9 (2), 460. doi:10.3390/jcm9020460

Jordão, J. F., Ayala-Grosso, C. A., Markham, K., Huang, Y., Chopra, R., McLaurin, J., et al. (2010). Antibodies targeted to the brain with image-guided focused ultrasound reduces amyloid-β plaque load in the TgCRND8 mouse model of alzheimer's disease. *PloS one* 5 (5), e10549. doi:10.1371/journal.pone.0010549

Kabalnov, A., Klein, D., Pelura, T., Schutt, E., and Weers, J. (1998). Dissolution of multicomponent microbubbles in the bloodstream: 1. Theory. *Ultrasound Med. Biol.* 24 (5), 739–749. doi:10.1016/s0301-5629(98)00034-9

Kawabata, K., Sugita, N., Yoshikawa, H., Azuma, T., and Umemura, S. (2005). Nanoparticles with multiple perfluorocarbons for controllable ultrasonically induced phase shifting. *Jpn. J. Appl. Phys.* 44 (6S), 4548. doi:10.1143/jjap.44.4548

Kee, A. L. Y., and Teo, B. M. (2019). Biomedical applications of acoustically responsive phase shift nanodroplets: current status and future directions. *Ultrason. Sonochem* 56, 37–45. doi:10.1016/j.ultsonch.2019.03.024

Khokhlova, V. A., Fowlkes, J. B., Roberts, W. W., Schade, G. R., Xu, Z., Khokhlova, T. D., et al. (2015). Histotripsy methods in mechanical disintegration of tissue: towards clinical applications. *Int. J. Hyperth.* 31 (2), 145–162. doi:10.3109/02656736.2015.1007538

Kim, J., DeRuiter, R. M., Goel, L., Xu, Z., Jiang, X., and Dayton, P. A. (2020). A comparison of sonothrombolysis in aged clots between low-boiling-point phase-change nanodroplets and microbubbles of the same composition. *Ultrasound Med. Biol.* 46 (11), 3059–3068. doi:10.1016/j.ultrasmedbio.2020.07.008

Kim, J., Lindsey, B. D., Chang, W., Dai, X., Stavas, J. M., Dayton, P. A., et al. (2017). Intravascular forward-looking ultrasound transducers for microbubble-mediated sonothrombolysis. *Sci. Rep.* 7 (1), 3454. doi:10.1038/s41598-017-03492-4

Kopechek, J. A., Carson, A. R., McTiernan, C. F., Chen, X., Hasjim, B., Lavery, L., et al. (2015). Ultrasound targeted microbubble destruction-mediated delivery of a transcription factor decoy inhibits STAT3 signaling and tumor growth. *Theranostics* 5 (12), 1378–1387. doi:10.7150/thno.12822

Kripfgans, O. D., Fabiilli, M. L., Carson, P. L., and Fowlkes, J. B. (2004). On the acoustic vaporization of micrometer-sized droplets. *J. Acoust. Soc. Am.* 116 (1), 272–281. doi:10.1121/1.1755236

Kripfgans, O. D., Fowlkes, J. B., Miller, D. L., Eldevik, O. P., and Carson, P. L. (2000). Acoustic droplet vaporization for therapeutic and diagnostic applications. *Ultrasound Med. Biol.* 26 (7), 1177–1189. doi:10.1016/s0301-5629(00)00262-3

Kripfgans, O. D., Fowlkes, J. B., Woydt, M., Eldevik, O. P., and Carson, P. L. (2002). *In vivo* droplet vaporization for occlusion therapy and phase aberration correction. *IEEE Trans. Ultrason. Ferroelectr. Freq. Control* 49 (6), 726–738. doi:10.1109/tuffc.2002.1009331

Kripfgans, O. D., Zhang, M., Fabiilli, M. L., Carson, P. L., Padilla, F., Swanson, S. D., et al. (2014). Acceleration of ultrasound thermal therapy by patterned acoustic droplet vaporization. *J. Acoust. Soc. Am.* 135 (1), 537–544. doi:10.1121/1.4828832

Lacour, T., Guédra, M., Valier-Brasier, T., and Coulouvrat, F. (2018). A model for acoustic vaporization dynamics of a bubble/droplet system encapsulated within a hyperelastic shell. *J. Acoust. Soc. Am.* 143 (1), 23–37. doi:10.1121/1.5019467

Lanza, G. M., Wallace, K. D., Scott, M. J., Cacheris, W. P., Abendschein, D. R., Christy, D. H., et al. (1996). A novel site-targeted ultrasonic contrast agent with broad biomedical application. *Circulation* 94 (12), 3334–3340. doi:10.1161/01.cir.94.12.3334

Lea-Banks, H., and Hynynen, K. (2021). Sub-millimetre precision of drug delivery in the brain from ultrasound-triggered nanodroplets. *J. Control. Release* 338, 731–741. doi:10.1016/j.jconrel.2021.09.014

Lea-Banks, H., Meng, Y., Wu, S., Belhadjhamida, R., Hamani, C., and Hynynen, K. (2021). Ultrasound-sensitive nanodroplets achieve targeted neuromodulation. *J. Control. Release* 332, 30–39. doi:10.1016/j.jconrel.2021.02.010

Lea-Banks, H., O'reilly, M. A., and Hynynen, K. (2019). Ultrasound-responsive droplets for therapy: a review. *J. Control. Release* 293, 144–154.

Lee, J., Carugo, D., Crake, C., Owen, J., de Saint Victor, M., Seth, A., et al. (2015). Nanoparticle-loaded protein–polymer nanodroplets for improved stability and conversion efficiency in ultrasound imaging and drug delivery. *Adv. Mater* 27 (37), 5484–5492. doi:10.1002/adma.201502022

Li, D. S., Kripfgans, O. D., Fabiilli, M. L., Brian Fowlkes, J., and Bull, J. L. (2014). Initial nucleation site formation due to acoustic droplet vaporization. *Appl. Phys. Lett.* 104 (6), 063703. doi:10.1063/1.4864110

Li, Y., Liu, R., Liu, L., Zhang, Y., Sun, J., Ma, P., et al. (2020). Study on phase transition and contrast-enhanced imaging of ultrasound-responsive nanodroplets with polymer shells. *Colloids Surfaces B Biointerfaces* 189, 110849. doi:10.1016/j.colsurfb.2020.110849

Lin, S., Zhang, G., Jamburidze, A., Chee, M., Leow, C. H., Garbin, V., et al. (2018). Imaging of vaporised sub-micron phase change contrast agents with high frame rate ultrasound and optics. *Phys. Med. and Biol.* 63 (6), 065002. doi:10.1088/1361-6560/aaac05

Lin, S., Zhang, G., Jamburidze, A., Chee, M., Leow, V., C. H., Garbin, M.-T., et al. (2017b). High frame rate ultrasound imaging of vaporised phase change contrast agents. *IEEE Int. Ultrason. Symp. (IUS)*, 1–3. doi:10.1109/ultsym.2017.8091521

Lin, S., Zhang, Ge, Leow, C. H., Matsunaga, T. O., and Tang, M.-X. (2016). Vaporising phase change ultrasound contrast agent in microvascular confinement. *IEEE Int. Ultrason. Symp. (IUS)*, 1–4. doi:10.1109/ultsym.2016.7728724

Lin, S., Zhang, G., Leow, C. H., and Tang, M. (2017a). Effects of microchannel confinement on acoustic vaporisation of ultrasound phase change contrast agents. *Phys. Med. and Biol.* 62 (17), 6884–6898. doi:10.1088/1361-6560/aa8076

Liu, H., Fan, C., Ting, C., and Yeh, C. (2014). Combining microbubbles and ultrasound for drug delivery to brain tumors: current progress and overview. *Theranostics* 4 (4), 432–444. doi:10.7150/thno.8074

Liu, J., Shang, T., Wang, F., Cao, Y., Hao, L., Ren, J., et al. (2017). Low-intensity focused ultrasound (LIFU)-induced acoustic droplet vaporization in phase-transition perfluoropentane nanodroplets modified by folate for ultrasound molecular imaging. *Int. J. nanomedicine* Vol. 12, 911–923. doi:10.2147/ijn.s122667

Lo, A. H., Kripfgans, O. D., Carson, P. L., Rothman, E. D., and Fowlkes, J. B. (2007). Acoustic droplet vaporization threshold: effects of pulse duration and contrast agent. *IEEE Trans. Ultrason. Ferroelectr. Freq. Control* 54 (5), 933–946. doi:10.1109/tuffc.2007.339

Loskutova, K., Grishenkov, D., and Ghorbani, M. (2019). Review on acoustic droplet vaporization in ultrasound diagnostics and therapeutics. *BioMed Res. Int.* 2019, 1–20. doi:10.1155/2019/9480193

Luke, G. P., Hannah, A. S., and Emelianov, S. Y. (2016). Super-resolution ultrasound imaging *in vivo* with transient laser-activated nanodroplets. *Nano Lett.* 16 (4), 2556–2559. doi:10.1021/acs.nanolett.6b00108

Maghsoudinia, F., Akbari-Zadeh, H., Aminolroayaei, F., Birgani, F. F., Shanei, A., and Samani, R. K. (2022). Ultrasound responsive Gd-DOTA/doxorubicin-loaded nanodroplet as a theranostic agent for magnetic resonance image-guided controlled release drug delivery of melanoma cancer. *Eur. J. Pharm. Sci.* 174, 106207. doi:10.1016/j.ejps.2022.106207

Mannaris, C., Bau, L., Grundy, M., Gray, M., Lea-Banks, H., Seth, A., et al. (2019). Microbubbles, nanodroplets and gas-stabilizing solid particles for ultrasound-mediated extravasation of unencapsulated drugs: an exposure parameter optimization study. *Ultrasound Med. Biol.* 45 (4), 954–967. doi:10.1016/j.ultrasmedbio.2018.10.033

Melich, R., Bussat, P., Morici, L., Vivien, A., Gaud, E., Bettinger, T., et al. (2020). Microfluidic preparation of various perfluorocarbon nanodroplets: characterization and determination of acoustic droplet vaporization (ADV) threshold. *Int. J. Pharm.* 587, 119651. doi:10.1016/j.ijpharm.2020.119651

Meng, D., Guo, L., Shi, D., Sun, X., Shang, M., Zhou, X., et al. (2019). Charge-conversion and ultrasound-responsive O-carboxymethyl chitosan nanodroplets for controlled drug delivery. *Nanomedicine* 14 (19), 2549–2565. doi:10.2217/nnm-2019-0217

Miles, C. J., Doering, C. R., and Kripfgans, O. D. (2016). Nucleation pressure threshold in acoustic droplet vaporization. *J. Appl. Phys.* 120 (3). doi:10.1063/1.4958907

Mitcham, T. M., Nevozhay, D., Chen, Y., Nguyen, L. D., Pinton, G. F., Lai, S. Y., et al. (2022). Effect of perfluorocarbon composition on activation of phase-changing ultrasound contrast agents. *Med. Phys.* 49 (4), 2212–2219. doi:10.1002/mp.15564

Moyer, L. C., Timbie, K. F., Sheeran, P. S., Price, R. J., Miller, G. W., and Dayton, P. A. (2015). High-intensity focused ultrasound ablation enhancement *in vivo* via phase-shift nanodroplets compared to microbubbles. *J. Ther. ultrasound* 3, 7–9. doi:10.1186/s40349-015-0029-4

Mozafari, M., Shimoda, M., Urbanska, A. M., and Laurent, S. (2016). Ultrasound-targeted microbubble destruction: toward a new strategy for diabetes treatment. *Drug Discov. Today* 21 (4), 540–543. doi:10.1016/j.drudis.2015.11.010

Navarro-Becerra, J. A., Song, K., Martinez, P., and Borden, M. A. (2022). Microbubble size and dose effects on pharmacokinetics. *ACS biomaterials Sci. and Eng.* 8 (4), 1686–1695. doi:10.1021/acsbiomaterials.2c00043

Ninomiya, K., Noda, K., Ogino, C., Kuroda, S., and Shimizu, N. (2014). Enhanced OH radical generation by dual-frequency ultrasound with TiO2 nanoparticles: its application to targeted sonodynamic therapy. *Ultrason. Sonochem* 21 (1), 289–294. doi:10.1016/j.ultsonch.2013.05.005

Overvelde, M., Garbin, V., Sijl, J., Dollet, B., De Jong, N., Lohse, D., et al. (2010). Nonlinear shell behavior of phospholipid-coated microbubbles. *Ultrasound Med. Biol.* 36 (12), 2080–2092. doi:10.1016/j.ultrasmedbio.2010.08.015

Pajek, D., Burgess, A., Huang, Y., and Hynynen, K. (2014). High-intensity focused ultrasound sonothrombolysis: the use of perfluorocarbon droplets to achieve clot lysis at reduced acoustic power. *Ultrasound Med. Biol.* 40 (9), 2151–2161. doi:10.1016/j.ultrasmedbio.2014.03.026

Paproski, R. J., Forbrich, A., Hitt, M., and Zemp, R. (2014). RNA biomarker release with ultrasound and phase-change nanodroplets. *Ultrasound Med. Biol.* 40 (8), 1847–1856. doi:10.1016/j.ultrasmedbio.2014.01.011

Park, J., Zhang, Y., Vykhodtseva, N., Jolesz, F. A., and McDannold, N. J. (2012). The kinetics of blood brain barrier permeability and targeted doxorubicin delivery into brain induced by focused ultrasound. *J. Control. Release* 162 (1), 134–142. doi:10.1016/j.jconrel.2012.06.012

Pellerito, J., and Polak, J. F. (2012). *Introduction to vascular ultrasonography: expert consult-online and print*. Elsevier Health Sciences.

Phillips, L. C., Puett, C., Sheeran, P. S., Dayton, P. A., Timbie, K. F., Price, R. J., et al. (2013a). Enhanced *in vivo* and *in vitro* high intensity focused ultrasound ablation via phase-shift nanodroplets compared to microbubbles. *IEEE Int. Ultrason. Symp. (IUS)*, 1821–1824. doi:10.1109/ultsym.2013.0464

Phillips, L. C., Puett, C., Sheeran, P. S., Dayton, P. A., Wilson Miller, G., and Matsunaga, T. O. (2013b). Phase-shift perfluorocarbon agents enhance high intensity focused ultrasound thermal delivery with reduced near-field heating. *J. Acoust. Soc. Am.* 134 (2), 1473–1482. doi:10.1121/1.4812866

Porter, T., and Zhang, P. (2008). Temperature and size-dependence of the vaporization threshold of phase-shift emulsions. *J. Acoust. Soc. Am.* 123 (5), 2997. doi:10.1121/1.2932552

Prepared by the Safety Group of the British Medical Ultrasound Society (2010). Guidelines for the safe use of diagnostic ultrasound equipment. *Ultrasound* 18 (2), 52–59. doi:10.1258/ult.2010.100003

Presset, A., Bonneau, C., Kazuyoshi, S., Nadal-Desbarats, L., Mitsuyoshi, T., Bouakaz, A., et al. (2020). Endothelial cells, first target of drug delivery using microbubble-assisted ultrasound. *Ultrasound Med. Biol.* 46 (7), 1565–1583. doi:10.1016/j.ultrasmedbio.2020.03.013

Prokop, A. F., Soltani, A., and Roy, R. A. (2007). Cavitational mechanisms in ultrasound-accelerated fibrinolysis. *Ultrasound Med. Biol.* 33 (6), 924–933. doi:10.1016/j.ultrasmedbio.2006.11.022

Puett, C., Phillips, L. C., Sheeran, P. S., and Dayton, P. A. (2013). *In vitro* parameter optimization for spatial control of focused ultrasound ablation when using low boiling point phase-change nanoemulsions. *J. Ther. Ultrasound* 1, 16–13. doi:10.1186/2050-5736-1-16

Puett, C., Sheeran, P. S., Rojas, J. D., and Dayton, P. A. (2014). Pulse sequences for uniform perfluorocarbon droplet vaporization and ultrasound imaging. *Ultrasonics* 54 (7), 2024–2033. doi:10.1016/j.ultras.2014.05.013

Pysz, M. A., Machtaler, S. B., Seeley, E. S., Lee, J. J., Brentnall, T. A., Rosenberg, J., et al. (2015). Vascular endothelial growth factor receptor type 2–targeted contrast-enhanced US of pancreatic cancer neovasculature in a genetically engineered mouse model: potential for earlier detection. *Radiology* 274 (3), 790–799. doi:10.1148/radiol.14140568

Qin, D., Zhang, L., Chang, N., Ni, P., Zong, Y., Bouakaz, A., et al. (2018). *In situ* observation of single cell response to acoustic droplet vaporization: membrane deformation, permeabilization, and blebbing. *Ultrason. Sonochem* 47, 141–150. doi:10.1016/j.ultsonch.2018.02.004

Qin, D., Zhang, L., Zhu, H., Chen, J., Wu, D., Bouakaz, A., et al. (2021a). A highly efficient one-for-all nanodroplet for ultrasound imaging-guided and cavitation-enhanced photothermal therapy. *IJN* Vol. 16, 3105–3119. doi:10.2147/ijn.s301734

Qin, D., Zou, Q., Lei, S., Wang, W., and Li, Z. (2021b). Predicting initial nucleation events occurred in a metastable nanodroplet during acoustic droplet vaporization. *Ultrason. Sonochem* 75, 105608. doi:10.1016/j.ultsonch.2021.105608

Rapoport, N. (2012). Phase-shift, stimuli-responsive perfluorocarbon nanodroplets for drug delivery to cancer. *Wiley Interdiscip. Rev. Nanomedicine Nanobiotechnology* 4 (5), 492–510. doi:10.1002/wnan.1176

Rapoport, N. (2016) "Drug-loaded perfluorocarbon nanodroplets for ultrasound-mediated drug delivery," in *Therapeutic ultrasound*, 221–241.

Rapoport, N., Payne, A., Dillon, C., Shea, J., Scaife, C., and Gupta, R. (2013). Focused ultrasound-mediated drug delivery to pancreatic cancer in a mouse model. *J. Ther. ultrasound* 1 (1), 11. doi:10.1186/2050-5736-1-11

Rapoport, N. Y., Kennedy, A. M., Shea, J. E., Scaife, C. L., and Nam, K. (2009). Controlled and targeted tumor chemotherapy by ultrasound-activated nanoemulsions/microbubbles. *J. Control. Release* 138 (3), 268–276. doi:10.1016/j.jconrel.2009.05.026

Reznik, N., Seo, M., Williams, R., Bolewska-Pedyczak, E., Lee, M., Matsuura, N., et al. (2012). Optical studies of vaporization and stability of fluorescently labelled perfluorocarbon droplets. *Phys. Med. and Biol.* 57 (21), 7205–7217. doi:10.1088/0031-9155/57/21/7205

Reznik, N., Shpak, O., Gelderblom, E. C., Williams, R., De Jong, N., Versluis, M., et al. (2013). The efficiency and stability of bubble formation by acoustic vaporization of submicron perfluorocarbon droplets. *Ultrasonics* 53 (7), 1368–1376. doi:10.1016/j.ultras.2013.04.005

Reznik, N., Williams, R., and Burns, P. N. (2011). Investigation of vaporized submicron perfluorocarbon droplets as an ultrasound contrast agent. *Ultrasound Med. Biol.* 37 (8), 1271–1279. doi:10.1016/j.ultrasmedbio.2011.05.001

Riemer, K., Toulemonde, M., Yan, J., Lerendegui, M., Stride, E., Weinberg, P. D., et al. (2022). Fast and selective super-resolution ultrasound *in vivo* with acoustically activated nanodroplets. *IEEE Trans. Med. Imaging* 42 (4), 1056–1067. doi:10.1109/tmi.2022.3223554

Rojas, J. D., Borden, M. A., and Dayton, P. A. (2019). Effect of hydrostatic pressure, boundary constraints and viscosity on the vaporization threshold of low-boiling-point phase-change contrast agents. *Ultrasound Med. Biol.* 45 (4), 968–979. doi:10.1016/j.ultrasmedbio.2018.11.006

Sarkar, K., Katiyar, A., and Jain, P. (2009). Growth and dissolution of an encapsulated contrast microbubble: effects of encapsulation permeability. *Ultrasound Med. Biol.* 35 (8), 1385–1396. doi:10.1016/j.ultrasmedbio.2009.04.010

Schad, K. C., and Hynynen, K. (2010). *In vitro* characterization of perfluorocarbon droplets for focused ultrasound therapy. *Phys. Med. and Biol.* 55 (17), 4933–4947. doi:10.1088/0031-9155/55/17/004

Sen, T., Tufekcioglu, O., and Koza, Y. (2015). Mechanical index. *Anatol. J. Cardiol.* 15 (4), 334–336. doi:10.5152/akd.2015.6061

Sheeran, P. S., and Dayton, P. A. (2012). Phase-change contrast agents for imaging and therapy. *Curr. Pharm. Des.* 18 (15), 2152–2165. doi:10.2174/138161212800099883

Sheeran, P. S., and Dayton, P. A. (2014). Improving the performance of phase-change perfluorocarbon droplets for medical ultrasonography: current progress, challenges, and prospects. *Scientifica* 2014, 1–24. doi:10.1155/2014/579684

Sheeran, P. S., Luois, S., Dayton, P. A., and Matsunaga, T. O. (2011a). Formulation and acoustic studies of a new phase-shift agent for diagnostic and therapeutic ultrasound. *Langmuir* 27 (17), 10412–10420. doi:10.1021/la2013705

Sheeran, P. S., Luois, S. H., Mullin, L. B., Matsunaga, T. O., and Dayton, P. A. (2012). Design of ultrasonically-activatable nanoparticles using low boiling point perfluorocarbons. *Biomaterials* 33 (11), 3262–3269. doi:10.1016/j.biomaterials.2012.01.021

Sheeran, P. S., Matsunaga, T. O., and Dayton, P. A. (2013a). Phase change events of volatile liquid perfluorocarbon contrast agents produce unique acoustic signatures. *Phys. Med. and Biol.* 59 (2), 379–401. doi:10.1088/0031-9155/59/2/379

Sheeran, P. S., Matsunaga, T. O., and Dayton, P. A. (2013b). Phase-transition thresholds and vaporization phenomena for ultrasound phase-change nanoemulsions assessed via high-speed optical microscopy. *Phys. Med. and Biol.* 58 (13), 4513–4534. doi:10.1088/0031-9155/58/13/4513

Sheeran, P. S., Matsuura, N., Borden, M. A., Williams, R., Matsunaga, T. O., Burns, P. N., et al. (2016). Methods of generating submicrometer phase-shift perfluorocarbon droplets for applications in medical ultrasonography. *IEEE Trans. Ultrason. Ferroelectr. Freq. Control* 64 (1), 252–263. doi:10.1109/tuffc.2016.2619685

Sheeran, P. S., Rojas, J. D., Puett, C., Hjelmquist, J., Arena, C. B., and Dayton, P. A. (2015). Contrast-enhanced ultrasound imaging and *in vivo* circulatory kinetics with low-boiling-point nanoscale phase-change perfluorocarbon agents. *Ultrasound Med. Biol.* 41 (3), 814–831. doi:10.1016/j.ultrasmedbio.2014.10.020

Sheeran, P. S., Wong, V. P., Luois, S., McFarland, R. J., Ross, W. D., Feingold, S., et al. (2011b). Decafluorobutane as a phase-change contrast agent for low-energy extravascular ultrasonic imaging. *Ultrasound Med. Biol.* 37 (9), 1518–1530. doi:10.1016/j.ultrasmedbio.2011.05.021

Shpak, O., Verweij, M., Vos, H. J., de Jong, N., Lohse, D., and Versluis, M. (2014). Acoustic droplet vaporization is initiated by superharmonic focusing. *Proc. Natl. Acad. Sci.* 111 (5), 1697–1702. doi:10.1073/pnas.1312171111

Simpson, D. H., Chin, C. T., and Burns, P. N. (1999). Pulse inversion Doppler: a new method for detecting nonlinear echoes from microbubble contrast agents. *IEEE Trans. Ultrason. Ferroelectr. Freq. Control* 46 (2), 372–382. doi:10.1109/58.753026

Singh, R., Husseini, G. A., and Pitt, W. G. (2012). Phase transitions of nanoemulsions using ultrasound: experimental observations. *Ultrason. Sonochem* 19 (5), 1120–1125. doi:10.1016/j.ultsonch.2012.02.005

Sirsi, S., and Borden, M. (2009). Microbubble compositions, properties and biomedical applications. *Bubble Sci. Eng. Technol.* 1 (1-2), 3–17. doi:10.1179/175889709x446507

Sirsi, S., Feshitan, J., Kwan, J., Homma, S., and Borden, M. (2010). Effect of microbubble size on fundamental mode high frequency ultrasound imaging in mice. *Ultrasound Med. Biol.* 36 (6), 935–948. doi:10.1016/j.ultrasmedbio.2010.03.015

Sk, H., Monsky, W. L., Yuan, F., Roberts, W. G., Griffith, L., Torchilin, V. P., et al. (1998). Regulation of transport pathways in tumor vessels: role of tumor type and microenvironment. *Proc. Natl. Acad. Sci. U. S. A.* 95, 4607–4612. doi:10.1073/pnas.95.8.4607

Song, R., Zhang, C., Teng, F., Tu, J., Guo, X., Fan, Z., et al. (2021). Cavitation-facilitated transmembrane permeability enhancement induced by acoustically vaporized nanodroplets. *Ultrason. Sonochem* 79, 105790. doi:10.1016/j.ultsonch.2021.105790

Song, X., Feng, L., Liang, C., Yang, K., and Liu, Z. (2016). Ultrasound triggered tumor oxygenation with oxygen-shuttle nanoperfluorocarbon to overcome hypoxia-associated resistance in cancer therapies. *Nano Lett.* 16 (10), 6145–6153. doi:10.1021/acs.nanolett.6b02365

Spatarelu, C., Jandhyala, S., and Luke, G. P. (2023). Dual-drug loaded ultrasound-responsive nanodroplets for on-demand combination chemotherapy. *Ultrasonics* 133, 107056. doi:10.1016/j.ultras.2023.107056

Stride, E. P., and Coussios, C. C. (2010). Cavitation and contrast: the use of bubbles in ultrasound imaging and therapy. *Proc. Inst. Mech. Eng. Part H. J. Eng. Med.* 224 (2), 171–191. doi:10.1243/09544119jeim622

Strohm, E. M., Gorelikov, I., Matsuura, N., and Kolios, M. C. (2012). Acoustic and photoacoustic characterization of micron-sized perfluorocarbon emulsions. *J. Biomed. Opt.* 17 (9), 0960161. doi:10.1117/1.jbo.17.9.096016

Sutton, J. T., Ivancevich, N. M., Perrin, Jr S. R., Vela, D. C., and Holland, C. K. (2013). Clot retraction affects the extent of ultrasound-enhanced thrombolysis in an Ex Vivo porcine thrombosis model. *Ultrasound Med. Biol.* 39 (5), 813–824. doi:10.1016/j.ultrasmedbio.2012.12.008

Thermal ablation. *Seminars in roentgenology*: Elsevier; 2011.

Toprakcioglu, Z., Challa, P. K., Morse, D. B., and Knowles, T. (2020). Attoliter protein nanogels from droplet nanofluidics for intracellular delivery. *Sci. Adv.* 6 (6), eaay7952. doi:10.1126/sciadv.aay7952

Toulemonde, M., Harput, S., Tiennot, T., Zhou, X., and Tang, M.-X. (2020). 3D super localized flow with locally and acoustically activated nanodroplets and high frame rate imaging using a matrix array. *IEEE Int. Ultrason. Symp. (IUS)*, 1–4. doi:10.1109/ius46767.2020.9251319

Toulemonde, M., Zhang, G., Eckersley, R. J., and Tang, M.-X. (2018). Flow visualization through locally activated nanodroplets and high frame rate imaging. *IEEE Int. Ultrason. Symp. (IUS)*, 1–4. doi:10.1109/ultsym.2018.8579657

Yoon, H. (2018). Ultrasound and photoacoustic imaging of laser-activated phase-change perfluorocarbon nanodroplets. *Photonics* 8 (10), 405.

Van Namen, A., Jandhyala, S., Jordan, T., and Luke, G. P. (2021). Repeated acoustic vaporization of perfluorohexane nanodroplets for contrast-enhanced ultrasound imaging. *IEEE Trans. Ultrason. Ferroelectr. Freq. Control* 68 (12), 3497–3506. doi:10.1109/tuffc.2021.3093828

Vlaisavljevich, E., Aydin, O., Durmaz, Y. Y., Lin, K., Fowlkes, B., ElSayed, M., et al. (2015b). Effects of ultrasound frequency on nanodroplet-mediated histotripsy. *Ultrasound Med. Biol.* 41 (8), 2135–2147. doi:10.1016/j.ultrasmedbio.2015.04.007

Vlaisavljevich, E., Aydin, O., Durmaz, Y. Y., Lin, K., Fowlkes, B., Xu, Z., et al. (2016). Effects of droplet composition on nanodroplet-mediated histotripsy. *Ultrasound Med. Biol.* 42 (4), 931–946. doi:10.1016/j.ultrasmedbio.2015.11.027

Vlaisavljevich, E., Aydin, O., Lin, K., Durmaz, Y. Y., Fowlkes, B., ElSayed, M., et al. (2015c). The role of positive and negative pressure on cavitation nucleation in nanodroplet-mediated histotripsy. *Phys. Med. and Biol.* 61 (2), 663–682. doi:10.1088/0031-9155/61/2/663

Vlaisavljevich, E., Durmaz, Y. Y., Maxwell, A., Elsayed, M., and Xu, Z. (2013). Nanodroplet-mediated histotripsy for image-guided targeted ultrasound cell ablation. *Theranostics* 3 (11), 851–864. doi:10.7150/thno.6717

Vlaisavljevich, E., Lin, K., Maxwell, A., Warnez, M. T., Mancia, L., Singh, R., et al. (2015a). Effects of ultrasound frequency and tissue stiffness on the histotripsy intrinsic threshold for cavitation. *Ultrasound Med. Biol.* 41 (6), 1651–1667. doi:10.1016/j.ultrasmedbio.2015.01.028

Wang, C., Kang, S., and Yeh, C. (2013). Superparamagnetic iron oxide and drug complex-embedded acoustic droplets for ultrasound targeted theranosis. *Biomaterials* 34 (7), 1852–1861. doi:10.1016/j.biomaterials.2012.11.037

Welch, P. J., Li, D. S., Forest, C. R., Pozzo, L. D., and Shi, C. (2022). Perfluorocarbon nanodroplet size, acoustic vaporization, and inertial cavitation affected by lipid shell composition *in vitro*. *J. Acoust. Soc. Am.* 152 (4), 2493–2504. doi:10.1121/10.0014934

Williams, R., Wright, C., Cherin, E., Reznik, N., Lee, M., Gorelikov, I., et al. (2013). Characterization of submicron phase-change perfluorocarbon droplets for extravascular ultrasound imaging of cancer. *Ultrasound Med. Biol.* 39 (3), 475–489. doi:10.1016/j.ultrasmedbio.2012.10.004

Wilson, K. E., Wang, T. Y., and Willmann, J. K. (2013). Acoustic and photoacoustic molecular imaging of cancer. *J. Nucl. Med.* 54 (11), 1851–1854. doi:10.2967/jnumed.112.115568

Wong, Z. Z., Kripfgans, O. D., Qamar, A., Fowlkes, J. B., and Bull, J. L. (2011). Bubble evolution in acoustic droplet vaporization at physiological temperature via ultra-high speed imaging. *Soft Matter* 7 (8), 4009–4016. doi:10.1039/c1sm00007a

Wright, C. C., Hynynen, K., and Goertz, D. E. (2011). Pulsed focused ultrasound-induced displacements in confined *in vitro* blood clots. *IEEE Trans. Biomed. Eng.* 59 (3), 842–851. doi:10.1109/tbme.2011.2180904

Wu, J., Leong-Poi, H., Bin, J., Yang, L., Liao, Y., Liu, Y., et al. (2011). Efficacy of contrast-enhanced US and magnetic microbubbles targeted to vascular cell adhesion molecule–1 for molecular imaging of atherosclerosis. *Radiology* 260 (2), 463–471. doi:10.1148/radiol.11102251

Wu, Q., Mannaris, C., May, J. P., Bau, L., Polydorou, A., Ferri, S., et al. (2021). Investigation of the acoustic vaporization threshold of lipid-coated perfluorobutane nanodroplets using both high-speed optical imaging and acoustic methods. *Ultrasound Med. Biol.* 47 (7), 1826–1843. doi:10.1016/j.ultrasmedbio.2021.02.019

Wu, S., Fix, S. M., Arena, C. B., Chen, C. C., Zheng, W., Olumolade, O. O., et al. (2018). Focused ultrasound-facilitated brain drug delivery using optimized nanodroplets: vaporization efficiency dictates large molecular delivery. *Phys. Med. and Biol.* 63 (3), 035002. doi:10.1088/1361-6560/aaa30d

Xu, T., Cui, Z., Li, D., Cao, F., Xu, J., Zong, Y., et al. (2020). Cavitation characteristics of flowing low and high boiling-point perfluorocarbon phase-shift nanodroplets during focused ultrasound exposures. *Ultrason. Sonochem* 65, 105060. doi:10.1016/j.ultsonch.2020.105060

Xu, X., Ho, W., Zhang, X., Bertrand, N., and Farokhzad, O. (2016). Cancer nanomedicine: from targeted delivery to combination therapy. *Trends Mol. Med.* 21 (4), 223–232. doi:10.1016/j.molmed.2015.01.001

Xu, Z., Hall, T. L., Vlaisavljevich, E., and Lee, Jr F. T. (2021). Histotripsy: the first noninvasive, non-ionizing, non-thermal ablation technique based on ultrasound. *Int. J. Hyperth.* 38 (1), 561–575. doi:10.1080/02656736.2021.1905189

Yarmoska, S. K., Yoon, H., and Emelianov, S. Y. (2019). Lipid shell composition plays a critical role in the stable size reduction of perfluorocarbon nanodroplets. *Ultrasound Med. Biol.* 45 (6), 1489–1499. doi:10.1016/j.ultrasmedbio.2019.02.009

Yoo, K., Walker, W. R., Williams, R., Tremblay-Darveau, C., Burns, P. N., and Sheeran, P. S. (2018). Impact of encapsulation on *in vitro* and *in vivo* performance of volatile nanoscale phase-shift perfluorocarbon droplets. *Ultrasound Med. Biol.* 44 (8), 1836–1852. doi:10.1016/j.ultrasmedbio.2018.04.015

Yu, J., Chen, X., Villanueva, F. S., and Kim, K. (2016). Vaporization and recondensation dynamics of indocyanine green-loaded perfluoropentane droplets irradiated by a short pulse laser. *Appl. Phys. Lett.* 109 (24). doi:10.1063/1.4972184

Zhang, G., Harput, S., Hu, H., Christensen-Jeffries, K., Zhu, J., Brown, J., et al. (2018b). Fast acoustic wave sparsely activated localization microscopy (Fast-AWSALM) using octafluoropropane N anodroplets. *IEEE Int. Ultrason. Symp. (IUS)*, 1–9. doi:10.1109/ultsym.2018.8580192

Zhang, G., Harput, S., Lin, S., Christensen-Jeffries, K., Leow, C. H., Brown, J., et al. (2018a). Acoustic wave sparsely activated localization microscopy (AWSALM): super-resolution ultrasound imaging using acoustic activation and deactivation of nanodroplets. *Appl. Phys. Lett.* 113 (1). doi:10.1063/1.5029874

Zhang, G., Harput, S., Shah, A., Hernández-Gil, J., Zhu, J., Christensen-Jeffries, K.., et al. (2019c). Photoacoustic super-resolution imaging using laser activation of low-boiling-point dye-coated nanodroplets *in vitro* and *in vivo*. *IEEE Int. Ultrason. Symp. (IUS)*, 944–947. doi:10.1109/ultsym.2019.8926179

Zhang, G., Liao, C., Hu, J., Hu, H., Lei, Y., Harput, S., et al. (2023b). Nanodroplet-based super-resolution ultrasound localization microscopy. *ACS sensors* 8 (9), 3294–3306. doi:10.1021/acssensors.3c00418

Zhang, G., Lin, S., Leow, C. H., Pang, K., Hernández-Gil, J., Chee, M., et al. (2017b). Acoustic response of targeted nanodroplets post-activation using high frame rate imaging. *IEEE Int. Ultrason. Symp. (IUS)*, 1–4. doi:10.1109/ultsym.2017.8092693

Zhang, G., Lin, S., Leow, C. H., Pang, K. T., Hernández-Gil, J., Long, N. J., et al. (2019a). Quantification of vaporised targeted nanodroplets using high-frame-rate ultrasound and optics. *Ultrasound Med. Biol.* 45 (5), 1131–1142. doi:10.1016/j.ultrasmedbio.2019.01.009

Zhang, G., Toulemonde, M., Riemer, K., Zhu, J., Harput, S., Christensen-Jeffries, K., et al. (2020). *Effects of mechanical index on repeated sparse activation of nanodroplets in vivo*, 1–4.

Zhang, G., Wang, B., Shah, A., Bamber, J., and Tang, M.-X. (2019b). Contrast-enhanced photoacoustic imaging of low-boiling-point phase-change nanodroplets. *IEEE Int. Ultrason. Symp. (IUS)*, 2271–2274. doi:10.1109/ultsym.2019.8925633

Zhang, G., Yu, J., Lei, Y., Hu, J., Hu, H., Harput, S., et al. (2022b). Ultrasound super-resolution imaging for the differential diagnosis of thyroid nodules: a pilot study. *Front. Oncol.* 12, 978164. doi:10.3389/fonc.2022.978164

Zhang, M., Fabiilli, M. L., Haworth, K. J., Fowlkes, J. B., Kripfgans, O. D., Roberts, W. W., et al. (2010). Initial investigation of acoustic droplet vaporization for occlusion in canine kidney. *Ultrasound Med. Biol.* 36 (10), 1691–1703. doi:10.1016/j.ultrasmedbio.2010.06.020

Zhang, P., and Porter, T. (2010). An *in vitro* study of a phase-shift nanoemulsion: a potential nucleation agent for bubble-enhanced HIFU tumor ablation. *Ultrasound Med. Biol.* 36 (11), 1856–1866. doi:10.1016/j.ultrasmedbio.2010.07.001

Zhang, Q., Yang, Y., Xue, H., Zhang, H., Yuan, Z., Shen, Y., et al. (2023c). Intensified and controllable vaporization of phase-changeable nanodroplets induced by simultaneous exposure of laser and ultrasound. *Ultrason. Sonochem* 94, 106312. doi:10.1016/j.ultsonch.2023.106312

Zhang, W., Metzger, H., Vlatakis, S., Claxton, A., Carbajal, M. A., Fung, L. F., et al. (2023a). Characterising the chemical and physical properties of phase-change nanodroplets. *Ultrason. Sonochem* 97, 106445. doi:10.1016/j.ultsonch.2023.106445

Zhang, W., Shi, Y., Abd Shukor, S., Vijayakumaran, A., Vlatakis, S., Wright, M., et al. (2022a). Phase-shift nanodroplets as an emerging sonoresponsive nanomaterial for imaging and drug delivery applications. *Nanoscale* 14 (8), 2943–2965. doi:10.1039/d1nr07882h

Zhang, X., Hu, J., Zhao, G., Huang, N., Tan, Y., Pi, L., et al. (2017a). PEGylated PLGA-based phase shift nanodroplets combined with focused ultrasound for blood brain barrier opening in rats. *Oncotarget* 8 (24), 38927–38936. doi:10.18632/oncotarget.17155

Zhang, X., Owens, G. E., Cain, C. A., Gurm, H. S., Macoskey, J., and Xu, Z. (2016). Histotripsy thrombolysis on retracted clots. *Ultrasound Med. Biol.* 42 (8), 1903–1918. doi:10.1016/j.ultrasmedbio.2016.03.027

Zhao, Y., Yue, P., Peng, Y., Sun, Y., Chen, X., Zhao, Z., et al. (2023). Recent advances in drug delivery systems for targeting brain tumors. *Drug Deliv.* 30 (1), 1–18. doi:10.1080/10717544.2022.2154409

Zhu, J., Wang, Z., Xu, X., Xu, M., Yang, X., Zhang, C., et al. (2020). Polydopamine-encapsulated perfluorocarbon for ultrasound contrast imaging and photothermal therapy. *Mol. Pharm.* 17 (3), 817–826. doi:10.1021/acs.molpharmaceut.9b01070